Climate Dynamics manuscript No.
(will be inserted by the editor)

The respective roles of surface temperature driven feedbacks and tropospheric adjustment to CO_2 in CMIP5 transient climate simulations

Lorenzo Tomassini · Olivier Geoffroy · Jean-Louis Dufresne · Abderrahmane Idelkadi · Chiara Cagnazzo · Karoline Block · Thorsten Mauritsen · Marco Giorgetta · Johannes Quaas

Received: date / Accepted: date

Abstract An overview of radiative climate feedbacks and ocean heat uptake efficiency diagnosed from idealized transient climate change experiments of 14 CMIP5 models is presented. Feedbacks explain about two times more variance in transient climate response across the models than ocean heat uptake efficiency. Cloud feedbacks can clearly be identified as the main source of inter-model spread. Models

Lorenzo Tomassini
Max Planck Institute for Meteorology, Hamburg, Germany
E-mail: lorenzo.tomassini@zmaw.de

O. Geoffroy
CNRM-GAME, Météo France, CNRS, Toulouse, France

J.-L. Dufresne
Laboratoire de Météorologie Dynamique, Istitut Pierre Simon Laplace (LMD/IPSL), Paris, France

A. Idelkadi
Laboratoire de Météorologie Dynamique, Istitut Pierre Simon Laplace (LMD/IPSL), Paris, France

C. Cagnazzo
Istituto di Scienze dell'Atmosfera e del Clima, CNR, Rome, Italy

K. Block
Max Planck Institute for Meteorology, Hamburg, Germany

T. Mauritsen
Max Planck Institute for Meteorology, Hamburg, Germany

M. Giorgetta
Max Planck Institute for Meteorology, Hamburg, Germany

J. Quaas
Meteorological Institute, University of Leipzig, Leipzig, Germany

with strong longwave feedbacks in the tropics feature substantial increases in cloud ice around the tropopause suggestive of changes in cloud-top heights. The lifting of the tropical tropopause goes together with a general weakening of the tropical circulation. Distinctive inter-model differences in cloud shortwave feedbacks occur in the subtropics including the equatorward flanks of the storm-tracks. Related cloud fraction changes are not confined to low clouds but comprise middle level clouds as well. A reduction in relative humidity through the lower and mid troposphere can be identified as being the main associated large-scale feature. Experiments with prescribed sea surface temperatures are analyzed in order to investigate whether the diagnosed feedbacks from the transient climate simulations contain a tropospheric adjustment component that is not conveyed through the surface temperature response. The strengths of the climate feedbacks computed from atmosphere-only experiments with prescribed increases in sea surface temperatures, but fixed CO_2 concentrations, are close to the ones derived from the transient experiment. Only the cloud shortwave feedback exhibits discernible differences which, however, can not unequivocally be attributed to tropospheric adjustment to CO_2. Although for some models a tropospheric adjustment component is present in the global mean shortwave cloud feedback, an analysis of spatial patterns does not lend support to the view that cloud feedbacks are dominated by their tropospheric adjustment part. Nevertheless, there is positive correlation between the strength of tropospheric adjustment processes and cloud feedbacks across different climate models.

Keywords Climate feedbacks · Tropospheric adjustment · Transient climate response

1 Introduction

Only about one third of the equilibrium surface temperature response to a doubling of the atmospheric CO_2 concentration is a direct consequence of the change in the CO_2 content. About two thirds are due to feedbacks in the climate system (e.g. Held and Soden 2000, Dufresne and Bony 2008, Langen et al 2012, Mauritsen et al 2012). Moreover, the direct forcing caused by the pure CO_2 concentration increase is quite consistently computed by the radiation schemes in various climate models. Although not negligible, it does not constitute the major source of inter-model spread (Myhre et al 1998, Collins et al 2006, Forster and Taylor 2006, Gettelman et al 2012).

Therefore, in order to understand the diverse sensitivities of climate models to greenhouse gas concentration changes, an analysis of the main feedbacks as simulated by the various models is fundamental (Manabe and Wetherald 1980, Hansen et al 1984, Wetherald and Manabe 1988, Cess and Potter 1988, Zhang et al 1994). This allows not only for identifying the sources of inter-model differences, but also for isolating key physical processes that are involved in robust model responses to CO_2 concentration changes, and consequently for a better understanding of the climate system. In transient climate change simulations, not only climate intrinsic feedbacks determine the surface temperature response, also the thermal inertia of the ocean plays a role (Dufresne and Bony 2008, Winton et al 2010).

In the traditional definition of radiative feedbacks, the feedback is a consequence of the change in surface temperature provoked by the forcing agent. The feedback in turn induces a perturbation in the radiative budget at the top of the atmosphere and thus reinforces or counteracts the effect of the forcing on the surface temperature. It is however not evident whether the radiative effects of changes in water vapor, clouds, or the atmospheric lapse rate, for instance, depend only on the surface temperature anomaly.

Gregory and Webb (2008) described a tropospheric adjustment to abrupt increases in the atmospheric CO_2 concentration which occurs even in the case when sea surface temperatures are held constant. According to their study, the surface dependent shortwave cloud feedback is statistically insignificant in nearly all the examined models, and radiative changes caused by clouds depend on the CO_2 concentration change rather than on the magnitude of the surface temperature perturbation.

This raises the question whether there are cloud feedbacks in the traditional sense at all, or if the changes in clouds are an effect of changed heating rates in the atmosphere, with consequent changes to stability, vertical mixing, and the moisture profile, which do not depend on the amplitude of the surface temperature anomalies (Gregory and Webb 2008).

Alternatively, as suggested by Colman and McAvaney (2011), tropospheric adjustment is confined to cloud fraction changes affecting the shortwave radiation budget, and relevant surface temperature dependent feedbacks are present in all cloud components. Similarly, Webb et al (2012) estimate that cloud feedbacks contribute about four times as much as the cloud changes caused by tropospheric adjustment to the range of climate sensitivity in an ensemble of climate model simulations. In this case one might ask if the strength of tropospheric adjustment processes and the amplitude of surface temperature driven cloud feedbacks are related.

It is not obvious whether tropospheric adjustment to abrupt alterations in CO_2 concentration as diagnosed from experiments with fixed sea surface temperatures (SSTs) is relevant for the case of transient climate change (Andrews et al 2011, Andrews et al 2012). In these types of atmosphere-only experiments, for technical reasons, land surface temperatures are not held constant but are allowed to change. A quadrupling of the CO_2 concentration with only sea surface temperatures held fixed causes rising motion and cloud cover at all levels to shift from ocean to land (Watanabe et al 2011, Kamae and Watanabe 2012, Wyant et al 2012). This effect however is mediated through surface warming and not supposed to be addressed as tropospheric adjustment in the strict sense. Under transient and equilibrium global warming, observed and modeled climates show a nearly time-invariant ratio of mean land to mean ocean surface temperature change (Lambert and Webb 2011). When climate is forced with increasing atmospheric CO_2 concentrations, heat is transported from the land to the ocean, constraining the land to warm in step with the ocean surface.

On the other hand, when climate is driven by prescribed changes in SSTs, the heat transport anomaly moves heat from ocean to land, warming the land surface (Lambert and Webb 2011). As a consequence, atmosphere-only simulations with prescribed SST anomalies show very similar land surface temperature changes as coupled climate model simulations forced by CO_2 changes that lead to similar SST perturbations. This brings up the issue, intimately linked to the question about the role of tropospheric adjustment, whether climate feedbacks diagnosed from fixed

SST experiments are identical to the ones inferred from fully coupled transient climate change simulations (Colman and McAvaney 1997, Gettelman et al 2012).

In order to appropriately address the question about the respective roles of tropospheric adjustment to CO_2 and surface temperature governed feedbacks in transient climate change, a set of idealized experiments as well as an ensemble of 14 different climate models are analyzed. The simulations are part of the fifth phase of the Coupled Model Intercomparison Project (CMIP5, Taylor et al 2012).

The article is structured as follows. In the second section the climate models and the experiments are introduced. In the third section the methods that are used to quantify the climate feedbacks, the partial radiative perturbation technique and the radiative kernel method, are described. Also the role of the radiation scheme involved in the feedback analysis is discussed.

The fourth section presents an overview of the various feedbacks in the ensemble of coupled climate models as diagnosed from a simulation in which the atmospheric CO_2 concentration is increased by 1 percent per year, starting from the pre-industrial control state until the CO_2 concentration reaches four times the pre-industrial value (termed "1pctCO2"). An estimate of the ocean heat uptake efficiency is given for all models, and the relative contribution of feedbacks and ocean heat uptake efficiency to the explanation of inter-model differences in the transient climate response is discussed.

In agreement with previous studies, the model spread in the combined water vapor and lapse rate feedback, as well as the albedo and Planck feedback, is found to be rather small (Colman 2003, Soden and Held 2006). Therefore, the feedbacks associated with clouds are identified as the major source of inter-model differences. Consequently the most important aspects of changes in cloud properties are examined in Section 4.2 in more detail, and the changes in cloud characteristics are related to alterations in large-scale diagnostic indices across the ensemble of climate models.

In section 5, climate feedbacks and top-of-the-atmosphere radiative perturbations in various AMIP-type experiments are investigated in order to assess the respective roles of surface temperature changes and tropospheric adjustment processes caused by the CO_2 increase. Experiments in which the SSTs are uniformly increased by 4 Kelvin (termed "amip4K"), as well as experiments in which a patterned SST perturbation is added (termed "amipFuture"), are compared to the standard present-day AMIP simulations. A comparison of the climate feedbacks in these experiments with the ones diagnosed from the "1pctCO2" simulation allows for attributing the amplitudes of various climate feedbacks to surface temperature anomalies. Similarly, top-of-the-atmosphere radiative fluxes in AMIP-type experiments with quadrupled atmospheric CO_2 concentration but fixed present-day SSTs (termed "amip4xCO2") are analyzed in order to examine the tropospheric adjustment to changes in CO_2.

Finally, the results of the paper are summarized in a set of conclusions.

2 Models and simulations

The feedback analysis is based on the idealized 1 % per year CO_2 increase experiment "1pctCO2" of CMIP5 (Taylor et al 2012). In this experiment the atmospheric CO_2 concentration is prescribed and increased by 1 % per year starting from the

Table 1 The coupled climate models considered in the present work, the name of their atmospheric and oceanic components, and the vertical and horizontal resolution of the atmospheric components.

coupled model	atmospheric part	oceanic part	vertical res	horizontal res
MPI-ESM-LR	ECHAM6	MPI-OM	47 levels	1.875x1.875 deg
MPI-ESM-MR	ECHAM6	MPI-OM TP04	95 levels	1.875x1.875 deg
CNRM-CM5	ARPEGE	NEMO v3.2	31 levels	1.4x1.4 deg
HadGEM2-ES	HadGEM2-A	HadGEM2-O	38 levels	1.25x1.875 deg
NorESM1-M	CAM4-Oslo	MICOM	26 levels	1.9x2.5 deg
IPSL-CM5A-LR	LMDZ5A	NEMO v3.2	39 levels	1.875x3.75 deg
ACCESS1-0	HadGEM2-A	GFDL MOM4.1	38 levels	1.25x1.875 deg
bcc-csm-1	BCC T63	IAP T63	16 levels	2.8125x2.8125 deg
CanESM2	CanAM4	CanOM4	35 levels	2.8125x2.8125 deg
inmcm4	inmcm4-A	inmcm4-O	21 levels	1.5x2.0 deg
MIROC5	CCSR-AGCM	COCO	40 levels	1.4x1.4 deg
MRI-CGCM3	MRI-AGCM3	MRI-COM3	35 levels	1.125x1.125 deg
CCSM4	CAM4	POP2	26 levels	0.94x1.125 deg
CESM1-CAM5	CAM5	POP2	30 levels	0.94x1.125 deg

year 1850 of a pre-industrial control simulation until quadrupling of the CO_2 concentration with respect to pre-industrial levels after 140 years. All other external forcings, in particular aerosols, are kept at their pre-industrial values.

In order to investigate the respective roles of surface temperature increases and tropospheric adjustment to changes in CO_2 in climate model responses, atmosphere-only simulations with prescribed SSTs, so-called AMIP-type experiments, are analyzed.

In the experiment "amip4xCO2", sea surface temperature and sea ice for the years 1979 to 2008 are prescribed while the CO_2 concentration is quadrupled with respect to pre-industrial levels. In the experiment "amip4K", a uniform anomaly of 4 Kelvin is added to the prescribed sea surface temperatures of the years 1979 to 2008. The CO_2 concentration is kept at the present-day value. Similarly, in the experiment "amipFuture", a patterned anomaly is added to the prescribed sea surface temperatures of the years 1979 to 2008. The anomaly pattern is derived from a composite of the CMIP3 ensemble of coupled climate model response at time of CO_2 quadrupling. For all these AMIP-type experiments, the standard AMIP experiment with prescribed sea surface temperatures and sea ice of the years 1979 to 2008, and present-day CO_2 concentration, serves as a reference. The described experiments are part of the CMIP5 protocol (Taylor et al 2012).

For the feedback analysis, 14 different global climate models are considered: MPI-ESM-LR and MPI-ESM-MR (Giorgetta et al 2012, Stevens et al 2012), CNRM-CM5 (Voldoire et al 2012), HadGEM2-ES (Jones et al 2011), NorESM1-M (Seland et al 2008), IPSL-CM5A-LR (Dufresne et al 2012), ACCESS1-0, bcc-csm1-1 (Climate System Modeling Division 2005), CanESM2 (Chylek et al 2011), inmcm4 (Volodin et al 2010), MIROC5 (Watanabe et al 2010), MRI-CGCM3 (Yukimoto et al 2011), CCSM4 (Gent et al 2011), CESM1-CAM5 (Gettelman et al 2012).

In Table 1 all coupled models, their atmospheric and oceanic parts, and the resolutions of the atmospheric model components are summarized.

Figure 1 shows the global mean temperature increase, relative to the pre-industrial control run, in the 140 years of the “1pctCO2” experiment for the 14 models considered in the present study.

3 Feedback quantification methods

Changing the CO_2 concentration of the atmosphere can conceptually be understood as applying an external radiative forcing F to the climate system at the top of the atmosphere. As a consequence of this forcing, the surface temperature T_S changes. This in turn leads to changes in other characteristics of the climate system like the amount and distribution of water vapor in the atmosphere, or the surface albedo of the Earth following alterations in ice and snow cover, which again modifies the radiative flux R at the top of the atmosphere.

One can therefore distinguish between the direct radiative forcing that is caused by the change in atmospheric CO_2 content, and the feedbacks that are a result of the subsequent surface temperature increase or decrease. Both forcing and feedbacks have an effect on the energy balance of the climate system at the top of the atmosphere.

Changes in the energy balance of the climate system can be summarized in the following zero-dimensional energy balance model:

$$\Delta R = F + \lambda \cdot \Delta T_S \tag{1}$$

where λ denotes the feedback factor, which is the rate of change of top-of-the-atmosphere radiative fluxes with respect to the global mean surface temperature T_S.

Under the assumption of additivity of the feedback processes, the feedback factor λ can be decomposed into the effect of different individual feedbacks as $\lambda = \lambda_T + \lambda_A + \lambda_W + \lambda_C$, where λ_T describes the effect of the temperature feedback, λ_A the effect of the albedo feedback, λ_W the effect of the water vapor feedback, and λ_C the effect of the cloud feedback. The temperature feedback can be further decomposed into the Planck feedback λ_P and the lapse rate feedback λ_{LR}, where λ_P assumes that the temperature change is uniform throughout the atmosphere, in accordance with the surface temperature change, and λ_{LR} takes into account the modification due to the vertical nonuniformity of the temperature anomaly. For the temperature feedback only the troposphere is considered in order not to include the effects of stratospheric adjustment.

A way of quantifying feedbacks that closely follows the above definition of radiative feedbacks is the partial radiative perturbation (PRP) method introduced by Wetherald and Manabe (1988) (see also Colman and McAvaney 1997, Colman 2003). Off-line radiative transfer calculations are used to estimate the effect of specific meteorological fields on the radiative flux at the top of the atmosphere. Under the assumption of additivity, each variable is substituted, one at a time, from an experiment or time period with higher CO_2 concentrations, the perturbed simulation, while all other variables that enter the radiation calculation are taken from the control experiment. In our case the control simulation is the first 6 years of the “1pctCO2” experiment, while the perturbed simulation corresponds to the last 6 years of the same experiment.

The feedback factor λ_x for the variable x (which could be water vapor, clouds, surface albedo, or temperature) is then calculated as ΔR_x divided by ΔT_S, where ΔR_x is the difference of the top-of the-atmosphere radiative flux calculated from (i) the variable x from the perturbed experiment and all other variables from the control experiment, and (ii) all variables from the control experiment. In the case of the lapse rate feedback, only the vertical temperature profile up to the tropopause is perturbed, stratospheric temperatures are taken from the control period.

Colman and McAvaney (1997) pointed out that the assumption that all fields that enter the radiation scheme are uncorrelated introduces biases. This can partially be overcome by applying the partial radiative perturbation calculation twice. In the first step, the so-called forward PRP computation, the perturbed fields of the various variables are substituted as already described into the control simulation. In a second step, the perturbed simulation is defined to be the control simulation, and vice versa. The final radiative perturbation estimate of the feedback parameters λ_x is then defined to be the mean over forward and backward PRP computations.

Full PRP calculations are computationally expensive and temporally high-resolution model output fields are required. Soden and Held (2006) suggested the use of radiative kernels to simplify the computations and at the same time avoid the problem of correlated input fields. The idea is to write λ_x as a product of two terms, one dependent on the radiative transfer, the other on the climatic response:

$$\lambda_x = \frac{\partial R}{\partial x} \cdot \frac{\partial x}{\partial T_S} = K_x \cdot \frac{\partial x}{\partial T_S} \qquad (2)$$

The radiative kernel K_x is derived using a specific radiative transfer code. For more details on the method we refer the reader to Soden and Held (2006) and Soden et al (2008). In the present study we use a radiative kernel for the model intercomparison, but perform full PRP computations in the case of three climate models in order to assess the accuracy of the kernel method. The employed radiative kernel is calculated as described in Block and Mauritsen (2012) with one exception. The kernel used here is the mean of two kernels: a forward kernel which uses the pre-industrial state as a base state, and a backward kernel which assumes an equilibrated $4 \times CO_2$ climate as the reference state. A similar averaging of kernels was suggested by Jonko et al (2012). A comparison and validation of kernels computed from different base states is included in Block and Mauritsen (2012). In the case of the kernel method, top-of-the-atmosphere radiative fluxes due to changes in cloud fields, and corresponding cloud feedbacks, are calculated as suggested in Soden et al (2008). In contrast to the direct calculation of cloud feedbacks in PRP computations as described above, cloud feedbacks are determined by adjusting the model-simulated change in cloud radiative forcing to account for cloud masking effects (see also Shell et al 2008 and Block and Mauritsen 2012 for more details). For computations of top-of-the-atmosphere radiative fluxes based on the kernel method, monthly mean data are used.

The PRP computations are based on 6 hourly climate model output using an off-line version of the ECHAM6 radiation code, which rests on the Rapid Radiative Transfer Model (RRTM, Clough et al 2005). In the case of one model, the CNRM-CM5, the PRP calculations are performed in addition with the native radiation code of the model. The shortwave radiation scheme employed in CNRM-CM5 is

Table 2 Comparison of global mean feedback values based on PRP calculations and the radiative kernel method for three climate models. In case of CNRM-CM5 the PRP calculations are performed with the ECHAM6 radiation scheme as well as the native radiation code of the model.

Method	Albedo	Water vapor	Lapse rate	Cloud LW	Cloud SW
MPI-ESM-LR					
Kernel	0.25	2.19	-0.99	0.51	0.39
PRP	0.23	2.23	-1.07	0.48	0.30
IPSL-CM5A-LR					
Kernel	0.19	2.35	-1.05	0.30	1.13
PRP	0.21	1.82	-0.84	0.14	0.91
CNRM-CM5A					
Kernel	0.36	1.82	-0.45	0.36	0.22
PRP	0.47	1.56	-0.47	0.30	0.00
PRP own rad	0.43	1.66	-0.50	0.30	0.00

based on Fouquart and Bonnel (1980), while the longwave part relies on the RRTM as well.

Table 2 summarizes global mean values of surface albedo, water vapor, lapse rate, cloud longwave, and cloud shortwave feedbacks for the three models. The two methods are in good agreement. Figure 2 shows a comparison for longwave radiative fluxes at the top of the atmosphere due to changes in clouds as derived from PRP calculations (left column) and the radiative kernel method (right column) for the same climate models. In both cases the first 6 years of the "1pctCO2" simulation serve as the reference period, while the last 6 years of the same simulation provide the perturbed state. For CNRM-CM5 both the PRP computation with the ECHAM6 radiation code (third row) as well as the native radiation scheme of the model is shown (fourth row). The same results for the corresponding top-of-the-atmosphere cloud shortwave fluxes are presented in Figure 3.

The differences between the feedbacks calculated using PRP and the radiative kernel are not negligible and of a similar order of magnitude as the total cloud feedback. This is due to the fact that various simplifying assumptions enter the kernel calculations, that the kernel is computed from one single model and to some extent base-state dependent. Nevertheless, not only global mean values of radiative fluxes are satisfactorily reproduced by the kernel method, also the patterns compare favorably with the PRP reference calculations. Moreover, the discrepancies that are introduced by the use of different radiation schemes in case of the CNRM-CM5 model turn out to be small. Therefore, the kernel method is concluded to be suited for the model intercomparison in the subsequent sections of the present study, while for other objectives more precise methods might need to be applied (Block and Mauritsen 2012).

4 Feedbacks in transient climate simulations of CMIP5 models

In this section an overview of the strength of different feedbacks in 14 CMIP5 global climate models is presented. A discussion of the degree to which the feedback analysis can explain the model spread in surface temperature responses due to the atmospheric CO_2 concentration increase is included.

The analysis is based on the CMIP5 "1pctCO2" experiment which prescribes an increase in the atmospheric CO_2 concentration by 1 % per year starting from the pre-industrial control simulation and assumes constant aerosol emissions of the year 1850 as in the pre-industrial control run. In transient climate change simulations the amplitude of the temperature responses in the models is controlled not only by the strength of the feedbacks, but also by the efficiency of the ocean heat uptake. As proposed by Gregory and Mitchell (1997) and discussed in Dufresne and Bony (2008), in transient simulations with only a modest departure from equilibrium the ocean heat uptake efficiency κ can be estimated based on equation (1) by

$$\kappa = -\frac{\Delta R}{\Delta T_S} \tag{3}$$

assuming that the top-of-the-atmosphere imbalance R in equation (1) is approximately equal to the ocean heat uptake.

In Section 4.1 we summarize the results of the feedback analysis and identify the cloud feedback as the main source of inter-model differences. Consequently, in Section 4.2 the main features of the disparity in the modeled changes of cloud characteristics are discussed in more detail, and the various cloud responses are related to changes in a few key large-scale indices.

4.1 Feedback and ocean heat uptake intercomparison

The amplitudes of the albedo, water vapor, lapse rate, joint water vapor and lapse rate, cloud longwave, cloud shortwave, total cloud, and Planck feedback for the 14 CMIP5 models are presented in the upper panel of Figure 4. The absolute values as well as the ranges across different models are comparable to the ones reported in earlier studies (Bony et al 2006, Soden et al 2008). The strong negative correlation between the water vapor and the lapse rate feedback, due to a prominent contribution of both feedbacks in the tropical upper troposphere, has been noted in earlier studies (Held and Soden 2000, Colman 2003, Soden and Held 2006, Held and Shell 2012).

Since the ranges of absolute values for the albedo, the Planck, and the joint water vapor and lapse rate feedbacks are rather narrow, the cloud feedback can clearly be identified as the major source of inter-model differences. In agreement with Colman (2003) there is a negative correlation of -0.39 between cloud longwave and cloud shortwave feedback reducing the spread of the total cloud feedback compared to the sum of the ranges of its longwave and shortwave components. The comparatively larger range for cloud feedbacks could partly be due to the use of a radiative kernel and the indirect computation of the cloud feedbacks via the cloud radiative effect and corrections from other feedbacks. However, as shown in Section 3, the computed cloud feedbacks based on the radiative kernel method agree well with the respective reference values obtained by PRP computations.

The range in the cloud shortwave component, and consequently in the total cloud feedback, is dominated by two models: IPSL-CM5A-LR with an unusually strong positive and inmcm4 with a distinct negative shortwave cloud feedback.

The strong shortwave cloud feedback of IPSL-CM5A-LR is discussed thoroughly in Brient and Bony (2012). Some aspects of low cloud feedbacks in the previous version of inmcm4, inmcm3.0, are reviewed in Clement et al (2009). The rather strong cloud shortwave feedback in CESM1-CAM5 is examined in Gettelman et al (2012) and traced back to a new shallow convection scheme which causes large midlatitude cloud feedback differences compared to CAM4. Some of these issues are taken on in the next section.

The estimates of ocean heat uptake efficiency as calculated based on equation (3) together with the total feedback factor, i.e. the sum over all individual feedback factors, and the temperature response of each model is displayed in the lower panel of Figure 4. The range of the total feedback factor is about three times as large as the range of the ocean heat uptake efficiency across the model ensemble. Based on a linear regression approach, the ocean heat uptake efficiency explains 0.25, the total feedback factor 0.55 of the total variance of the temperature signals. Consequently, as shown in Figure 5, the consideration of the ocean heat uptake efficiency helps to explain the spread in the transient climate response, although a part of the variance in the transient climate response remains unaccounted for by the two diagnostics. Apart from inaccuracies in the feedback calculations this could partly be due to a limited efficiency of certain feedbacks in creating surface temperature changes (Mauritsen et al 2012). For instance, the outlier IPSL-CM5A-LR in Figure 5 exhibits a large total feedback due to its strongly positive cloud feedback, but the implied temperature response is subdued.

4.2 Cloud feedback mechanisms

For the discussion of model differences in cloud feedbacks we focus on three climate models to illustrate and highlight the main characteristics of the disparities. These characteristics are not confined to the three selected models but are, to a greater or lesser extent, features of the whole climate model ensemble. The IPSL-CM5A-LR shows the strongest cloud shortwave feedback, CanESM2 the strongest cloud longwave feedback. In order to contrast these two extreme cases, we single out CCSM4 as well, which exhibits a weak shortwave as well as longwave feedback.

The first two rows of Figure 6 display the cloud shortwave and longwave feedbacks of the three models. One can see that the strongest differences across models in the longwave feedbacks occur in the tropical Pacific and Indian Ocean roughly between 20 South and 20 North.

For the discussion of the cloud shortwave feedback we concentrate on the area between the 25th and 50th degree of latitude in both hemispheres where IPSL-CM5A-LR features a strong positive shortwave feedback which is virtually absent in the other two models. Inter-model differences in cloud shortwave feedbacks are of similar magnitude in the tropical region 20 South to 20 North. However, in the tropics the processes underlying cloud shortwave feedbacks are strongly regime-dependent and a more in-depth analysis would be required in this case. The focus on the subtropics, in a wider sense, allows for highlighting the dominant role of cloud fraction changes for shaping the characteristic of cloud shortwave feedbacks in the different models (Zelinka et al 2012b).

In the following we will refer to the area of 20 South to 20 North loosely as the “tropics”, and the region between the 25th and 50th degree of latitude in both hemispheres as the "subtropics". The latter region includes the equatorward flanks of the storm-tracks. The bottom row of Figure 6 displays the zonal mean cloud fraction changes for the three climate models.

First the cloud longwave feedback is discussed. The two models with strong cloud longwave feedback, IPSL-CM5A-LR and CanESM2, show a strong increase in cloud fraction around the tropopause between 200hPa and 100hPa. This distinct increase is absent in CCSM4. Especially IPSL-CM5A-LR exhibits a decrease in cloud cover on both sides of the equator between 400hPa and 200hPa which tends to limit, but not suppress the longwave feedback. Figure 7 shows zonal mean changes in cloud liquid water (left column) and cloud ice (right column) for the three models. The most striking feature, present in both IPSL-CM5A-LR and CanESM2 but completely absent in CCSM4, is the strong increase in cloud ice between 300hPa and 100hPa. Also CCSM4 exhibits an increase in cloud liquid water between 600hPa and 300hPa, actually even stronger than the other two models. This would suggest an increase in optical thickness of the clouds and a strong positive cloud longwave feedback in CCSM4 if no clouds were above. A consequence of the cloud liquid water increase at mid levels is the negative cloud shortwave feedback of CCSM4 in the western tropical Pacific (Figure 6). But the strength of the tropical longwave cloud feedback is governed to a large extent by the changes in cloud ice around the tropopause due to rising cloud-top height (Zelinka et al 2012b, Crueger et al 2012). That the high-level cloud fraction changes significantly contribute to the radiative flux perturbations at the top of the atmosphere is backed by the partitioning of the cloud feedback in Zelinka et al (2012a) (see especially Figure 1 in Zelinka et al 2012a which documents the strong longwave radiative contribution of optically thick clouds above 200hPa).

Turning to the cloud shortwave feedback, a strongly positive cloud shortwave feedback in IPSL-CM5A-LR can be observed over the whole Atlantic, but in particular between 50 South to 25 South and 25 North to 50 North. The main cause of the positive cloud shortwave feedback is a strong reduction in cloud cover as shown in the bottom row of Figure 6. A detailed analysis of the processes that lead to this reduction is contained in Brient and Bony (2012). The cloud cover decrease is not confined to boundary layer clouds as often emphasized in the literature (e.g. Bony and Dufresne 2005, Soden and Vecchi 2011), but includes also middle level clouds, in agreement with Zelinka et al (2012a). The area of cloud cover decrease partly overlaps with the storm-track regions in the northern and the southern hemispheres. Gettelman et al (2012) identify an enhanced positive cloud shortwave feedback in the subtropical trade cumulus regions and the equatorward flanks of the storm-tracks in CAM5 compared to CAM4 as a main reason of the increased climate sensitivity of CAM5 (see the cloud shortwave feedbacks in Figure 4 for CCSM4 and CESM1-CAM5).

A drying of the planetary boundary layer in the subtropics is suggested by Figure 7 for IPSL-CM5A-LR leading to a reduction of low cloud cover (Brient and Bony 2012, Rieck et al 2012). The opposite signal can be observed for CCSM4 in many areas. In the tropics the cloud shortwave feedback tends to be a mirror of the cloud longwave feedback. In the tropical Pacific and Indian Ocean, for instance, the increase of in-cloud water in high clouds creates a positive longwave and a negative shortwave feedback (Colman et al 2001, Zelinka et al 2012b).

It is generally difficult to disentangle causes and effects of changes in cloud characteristics. Here we relate the strength of cloud feedbacks to a few important indices related to large-scale climatic conditions: changes in lower tropospheric stability, upward vertical wind at 500hPa, relative humidity at 500hPa and 200hPa, a convection index, and surface temperature. For consistency with the discussion above, to examine the cloud longwave feedback we confine the indices to the area 20S to 20N, and to investigate the cloud shortwave feedback the indices are calculated for the region between the 25th and 50th degree of latitude in both hemispheres. As in Tan et al (2012), the modified K-index proposed by Charba (1977) is chosen as a simple measure of deep convective instability:

$$\mathrm{K} = \frac{T_{1000} + T_{850}}{2} - T_{500} + \frac{T_{d,1000} + T_{d,850}}{2} - (T_{700} - T_{d,700}), \tag{4}$$

where T denotes temperature and T_d dewpoint temperature. The modified K-index combines the near-surface and 500hPa temperature difference, the near-surface dewpoint (a direct measure of low-level moisture content), and the 700hPa dewpoint depression (an indirect measure of the vertical extent of the moist layer). Lower tropospheric stability (LTS) is defined as the difference in potential temperature between the 700hPa and the 1000hPa level. All indices are restricted to ocean areas except for the upward vertical wind which includes also the land parts of the regions. Tan et al (2012) relate similar large-scale variables to cloud regimes based on data from the International Satellite Cloud Climatology Project (ISCCP).

For the cloud longwave feedback and the tropical region of 20 South to 20 North the results are displayed in Figure 8. The upward vertical wind decreases in all models indicating a general weakening of the tropical circulation (Vecchi and Soden 2007). The modified K-index most strongly correlates with cloud longwave feedbacks. The positive changes in the modified K-index reflect the increased sea surface temperatures and low-level moisture content in the various models.

The situation is different regarding the cloud shortwave feedback in the region 50 South to 25 South and 25 North to 50 North (Figure 9). The climate models show a general increase in lower tropospheric stability. This is in contrast to observational evidence regarding the relation between cloud shortwave feedback and LTS (Wood and Bretherton 2006, Clement et al 2009, Zhang et al 2009), but in accordance with the results of the multi-model study by Webb et al (2012). Moreover, the modest correlation between LTS and cloud shortwave feedback suggests that changes in LTS are not primarily responsible for the cloud fraction changes associated with the positive cloud shortwave feedback in most models. Instead, changes in relative humidity may explain the general decrease in cloud cover over subtropical regions in agreement with Sherwood et al (2010). A strong decrease of relative humidity in the mid troposphere, which correlates significantly with the cloud shortwave feedback, can be observed in all models. The computation of a bootstrap resampling 5-95% confidence interval for the correlation yields [-0.95,-0.5], i.e. although the actual correlation of -0.85 is to some extent due to a single model, the relationship proves to be robust across the wider model ensemble. The increase of relative humidity at higher levels of the atmosphere is associated with the general upward shift of the tropopause (Sherwood et al 2010).

5 The role of surface temperature and tropospheric adjustment to CO_2

In the traditional framework, feedbacks are conceptually understood as consequences of surface temperature perturbations. In transient climate change simulations, however, heating rates in the atmosphere due to the increased CO_2 concentration change and may alter stability and the vertical moisture profile. These effects can in turn have an impact on cloud properties and the radiative fluxes at the top of the atmosphere and therefore introduce a cloud component in the forcing (Gregory and Webb 2008, Colman and McAvaney 2011).

Here the respective roles of surface temperature increases and tropospheric adjustment processes in transient climate simulations are assessed based on two AMIP-type experiments. In the experiment "amip4K" a uniform increase of 4 Kelvin is added to the SSTs of the years 1979 to 2008, and in the experiment "amip4xCO2" the SSTs of the years 1979 to 2008 are prescribed but the atmospheric CO_2 concentration is quadrupled. For both of these simulations the standard AMIP experiment serves as a reference.

The two experiments allow for assessing the role of tropospheric adjustment in two ways. In the "amip4K" experiment the various feedbacks can be diagnosed and compared to the feedbacks as calculated from the transient "1pctCO2" simulation. Differences may be attributed to the missing CO_2 concentration increase in "amip4K". However, one has to keep in mind that also SSTs are different in "amip4K" compared to "1pctCO2", both the base state as well as the anomaly. In "amip4xCO2" the surface driven feedbacks are essentially suppressed and top-of-the-atmosphere radiative fluxes shed light on the radiative effects of the tropospheric adjustment in various components of the climate system. However, for technical reasons land surface temperatures are not held constant in this experiment. The effects of consequent land-sea contrasts are not supposed to be included in the definition of "tropospheric adjustment".

The upper panel in Figure 10 contains an overview of the various feedbacks as calculated based on the "amip4K" experiment for 8 different CMIP5 models. The middle panel again contains the feedback strengths as determined from the "1pctCO2" simulation (identical to the ones in Figure 4). By definition the albedo feedbacks in the "amip4K" simulations are smaller because sea ice cover is held constant. The lapse rate feedbacks are quite similar in the two experiments, and the joint lapse rate and water vapor feedbacks prove to be virtually identical in the two experimental setups. It reflects the fact that the vertical profile of temperature changes are very alike in the two experiments, although in "amip4K" the CO_2 concentration is kept at the control value. Also the cloud longwave feedbacks are hardly distinguishable. In accordance, zonal mean cloud fraction changes agree well in "amip4K" and "1pctCO2" (Figure 6 and Figure 14, bottom rows).

Slightly more pronounced differences can be observed in the cloud shortwave feedbacks. They tend to be larger in the "1pctCO2" simulations compared to the "amip4K" experiments. Several issues may play a certain role in this context: suppressed changes in sea ice in "amip4K" and associated surface flux anomalies, different sea surface temperature change patterns as well as surface temperature base states, and the absent change in CO_2 and concomitant tropospheric adjustment processes. Figure 11 displays the cloud shortwave feedback in the "amip4K" (left column) and the "1pctCO2" (right column) experiment for four of the models.

It is obvious that not only the amplitudes but also the patterns of the feedbacks in the two experiments agree rather well. A feature that is robust across all models can be identified over Northern Europe and Siberia. Here the cloud shortwave feedback is larger in the “1pctCO2” simulation compared to the “amip4K” experiment in all four models. The negative shortwave feedback in the Southern Ocean between 70 South and 50 South tends to be slightly stronger in “amip4K” than in “1pctCO2”.

In order to assess whether the discrepancies are attributable to the different sea surface temperature anomalies in “amip4K” compared to “1pctCO2”, the feedbacks are diagnosed also from the “amipFuture” experiment for the four models. In “amipFuture” the surface temperature change pattern is derived from a composite of the CMIP3 SST responses at time of CO_2 quadrupling and supposed to be similar to the SST perturbation in the “1pctCO2” experiment.

It turns out that the cloud shortwave feedbacks in “amip4K” and “amipFuture” are very similar. Figure 12 shows the difference between the cloud shortwave feedback in “1pctCO2” and “amip4K” (first column), and the difference between the cloud shortwave feedback in “1pctCO2” and “amipFuture” (second column). No robust and discernible influence of the different sea surface temperature anomaly patterns of “amip4K” and “amipFuture” on the cloud shortwave feedbacks can be identified.

The right column in Figure 12 contains the differences in surface temperatures between the first six years of the “1pctCO2” simulation and the standard AMIP experiment. The first six years of “1pctCO2” represent the base state for the “1pctCO2” feedback analysis, and the standard AMIP experiment serves as reference simulation for the other AMIP-type experiments. The base states could have a certain impact on the feedbacks in case the assumption of linearity is not exactly fulfilled (Dommenget 2012). The base state of the “1pctCO2” experiment tends to be colder because it represents a pre-industrial climate, while in the AMIP experiment the SSTs of the years 1979 to 2008 are prescribed. Sea surface temperature differences over the Southern Ocean do not seem to be the main cause for differences in cloud shortwave feedbacks between “1pctCO2” and “amip4K” in this region. Some models exhibit warmer SSTs in the base climate of the “1pctCO2” simulation along the sea-ice margins around Antarctica, but this does not generally translate into a corresponding pattern in the cloud shortwave feedback. In MPI-ESM-LR one might speculate that the warmer SSTs in the said area lead to a more positive cloud shortwave feedback in “1pctCO2” compared to “amip4K”. However, for CanAM4 the relation between sea surface temperature difference and difference in cloud shortwave feedback is reversed. Here colder sea surface temperatures relate to a more positive cloud shortwave feedback in “1pctCO2”.

Sea ice differences between “1pctCO2” and “amip4K” might have an impact on cloud shortwave feedbacks over Northern Europe and Siberia. The climate of this region is sensitive to sea ice distributions over the Arctic (e.g. Pethoukov and Semenov 2010). Also in the tropical Pacific the sea surface temperature differences of the two base states could play a certain role. Changes in cloud characteristics could depend non-linearly on surface temperatures and show a threshold behavior which may be set also by the base state (e.g. Del Genio and Kovari 2002).

The radiative pattern due to changes in clouds diagnosed in the “amip4xCO2” experiment is very consistent across different climate models (Figure 13). The inter-model differences lie mainly in the amplitude of the signal. It is striking that the spatial patterns of longwave radiative fluxes are almost an exact mirror of the shortwave flux patterns. As to be expected, tropical land areas show positive longwave radiative fluxes due to enhanced convergence and convection (Wyant et al 2012). In tropical and subtropical ocean regions the longwave feedback is mostly negative due to increased subsidence and associated reduction in cloud cover (Colman and McAvaney 2011, Wyant et al 2012, Kamae and Watanabe 2012). As discussed by Kamae and Watanabe (2012), a reduction in surface turbulent heat fluxes and increase in near-surface atmospheric stability result in a shallowing of the tropical marine boundary layer. Warming and drying by increased heating rates lead to the reduction in cloud cover (Kamae and Watanabe 2012).

In contrast to the results by Colman and McAvaney (2011), cloud fraction changes are not confined to the lower troposphere, but are strongest in the upper troposphere between 500hPa and 100hPa in a transect along the Equator between 5 South and 5 North (Figure 14 first row). The presence of the continents is clearly identifiable around 80W, 0E, and 120E. This indicates that land-sea contrasts in the amip4xCO2 experiment could affect in particular top-of-the-atmosphere longwave radiative fluxes due to changes in high clouds. Kamae and Watanabe (2012) investigate the role of land-sea contrast by the examination of an aqua-planet experiment with fixed SSTs and quadrupled CO_2, named “ape4xCO2”, using the model MIROC5. They show that the main effects of tropospheric adjustment are present in the “ape4xCO2” experiment as well. The land masses mainly govern the spatial distribution of cloud radiative effects. However, they suggest that in “ape4xCO2” the cloud longwave radiative effect is mainly due to cloud masking and not to increase in high-cloud amount as in “amip4xCO2”. Since in the present work cloud masking effects are removed, and since nevertheless longwave radiative flux anomalies at the top of the atmosphere attributed to cloud changes are present, it is not clear if one can disregard the effect of land-sea contrasts in “amip4xCO2”.

Along a transect at 45 South (more precisely, a mean over the area 50 South to 40 South is calculated) the cloud fraction changes near the surface are not consistent across different models (Figure 14 second row). The location of the most pronounced changes is model dependent to a certain degree. In MPI-ESM-LR and CanAM4 they occur mainly in the lower troposphere and are suggestive of a shallowing of the boundary layer (Wyant et al 2012, Kamae and Watanabe 2012). In IPSL-CM5A-LR the changes extend from the surface to the upper troposphere and are also at this latitude strongest at levels below the tropopause.

In the shortwave cloud component of “amip4xCO2” distinct positive values occur over Northern Europe and Siberia. Over this region part of the differences between the diagnosed feedbacks in the “amip4K” experiment compared to the “1pctCO2” simulation may stem from tropospheric adjustment processes (compare the first column of Figure 12 with the second column of Figure 13). Also in Central Africa, the tropical Pacific and Indian Ocean differences between cloud shortwave feedbacks in “amip4K” and “1pctCO2” could be due to tropospheric adjustment being absent in “amip4K”. Strongest evidence for such an interpretation is provided by the simulations with HadGEM2-A (Figure 12 and 13 third rows). Overall however it is difficult to distinctly identify a component in the cloud feedback, as derived from transient climate change simulations, that is attributable to tropospheric adjustment as diagnosed from the “amip4xCO2” experiment. Although cloud shortwave feedbacks in the global mean are somewhat smaller in "amip4K" than in "1pctCO2" for most models, the spatial pattern of the difference does not conform well to the radiative shortwave flux anomalies due to clouds in "amip4xCO2".

This can be quantified and summarized in a Taylor diagram (Figure 15). Here top-of-the-atmosphere radiative flux anomalies, both shortwave and longwave, due to changes in clouds are compared across different simulations for 6 models. The reference case is the "1pctCO2" experiment. Flux anomalies from "amip4K" and "amipFuture" are scaled by the ratio of the global mean surface temperature increase in the "1pctCO2" simulation and global mean surface temperature increases in the respective experiment. For some, but not all, models adding the radiative flux anomalies of "amip4xCO2" to the ones from "amip4K" improves the agreement with "1pctCO2" in terms of the variances of the flux anomalies. For no model, however, the pattern correlation with the radiative flux anomalies from "1pctCO2" increases discernibly when considering the sum of "amip4xCO2" and "amip4K".

The strength of the radiative flux anomalies in "amip4xCO2" due to clouds positively correlates in general with the amplitude of the corresponding cloud feedbacks as computed from the "1pctCO2" simulations (Figure 16). This indicates that the sensitivity of cloud properties to heating rate changes caused by alterations in the CO_2 concentration and to surface temperature changes is related in the models.

6 Conclusions

Climate feedbacks and top-of-the atmosphere radiative fluxes are analyzed for an ensemble of 14 climate models in different idealized experimental setups in order to investigate the respective roles of surface temperature controlled feedbacks and tropospheric adjustment processes due to changes in CO_2.

Partial radiative perturbation calculations are performed to assess the accuracy of top-of-the-atmosphere radiative fluxes due to different components of the climate system as diagnosed by a radiative kernel. Although the discrepancies are not unsubstantial in some cases, the agreement between radiative kernel results and PRP computations is in general satisfactorily not only in the global mean, but also regarding spatial characteristics. Therefore the radiative kernel is used for the subsequent investigation.

A comparison of climate feedbacks in idealized transient climate change simulations with 14 CMIP5 coupled climate models reveals that the spread in the albedo, the joint water vapor and lapse rate, as well as the Planck feedback is rather small. This implies, in agreement with earlier studies, that the cloud feedbacks are the main source of inter-model differences in the transient climate response to a CO_2 increase. Moreover, feedbacks contribute about two times as much as ocean heat uptake efficiency to explain these disparities.

Most accentuated inter-model differences in longwave cloud feedbacks are located in the tropics between 20 South and 20 North. Models with strong longwave cloud feedbacks in this region exhibit a substantial change in cloud ice around the tropopause. This supports the "Proportionately Higher Anvil Temperature" (PHAT) hypothesis (Zelinka and Hartmann 2010) and confirms the findings by

Zelinka et al (2012b), who identify the cloud-top feedback as the dominant contributor to the longwave cloud feedback in the tropics. Moreover, as shown in Zelinka et al (2012a), optically thick clouds at high altitudes of the atmosphere contribute heavily to top-of-the-atmosphere radiative longwave fluxes. The increase of in-cloud water content between 500hPa and 300hPa is not only a feature of models with strong cloud longwave feedback, but also of climate models with weak longwave cloud feedback in the tropics, suggesting that differences in cloud water changes at these levels of the atmosphere are not governing the inter-model spread in tropical cloud longwave feedbacks to first order. The change in cloud-top height is associated with the lifting of the tropical tropopause and occurs in conjunction with a general weakening of the tropical circulation.

Distinctive inter-model differences in cloud shortwave feedbacks occur in the subtropical region 50 South to 25 South and 25 North to 50 North. In this area the cloud shortwave feedback is mainly caused by cloud fraction changes. These cloud fraction changes are not confined to low clouds but affect middle level clouds as well, in agreement with results by Zelinka et al (2012a) who find that midlevel cloud changes cause positive shortwave cloud feedbacks that are 80% as large as those due to low clouds. Varying degrees of reduction in relative humidity through the lower and mid troposphere can be identified as being the main large-scale feature connected with the subtropical positive cloud shortwave feedbacks in the models (Sherwood et al 2010). They may partly be related to the Hadley cell expansion and poleward displacement of the zonal jets, but there is strong evidence that dynamical shifts alone can not explain the full signal (Sherwood et al 2010).

In order to investigate whether the diagnosed feedbacks from the transient climate change simulation "1pctCO2" contain a component that is a direct effect of the CO_2 concentration change, and not mediated through the surface temperature anomaly, different AMIP-type experiments are analyzed. The strengths of the climate feedbacks computed from the "amip4K" experiment turn out to be close to the ones derived from the "1pctCO2" simulation. Apart from the albedo feedbacks, which are to a large degree suppressed in "amip4K", only the cloud shortwave feedback exhibits discernible differences. The discrepancies can however not unequivocally be attributed to tropospheric adjustment processes as diagnosed from the "amip4xCO2" experiment.

For instance, over tropical land areas tropospheric adjustment as simulated in "amip4xCO2" is characterized by enhanced convergence and a consequent positive longwave and negative shortwave feedback. But the patterns of the cloud feedback differences between "amip4K" and "1pctCO2" do not show these features consistently, except for central Africa. One reason may lie in the fact that in transient climate simulations the heat transport anomaly moves heat from land to ocean, constraining the land to warm in step with the ocean surface (Lambert and Webb 2011). In the "amip4xCO2" experiment land-sea contrasts regulate the spatial pattern of tropospheric adjustment as discussed in Kamae and Watanabe (2012). Over Northern Europe and Siberia as well as the tropical Pacific and Indian Ocean tropospheric adjustment processes could play a role. However, in these regions the different control climates for "1pctCO2" and "amip4K" may partly be responsible for the discrepancies in the diagnosed cloud shortwave feedbacks, too. Over northern continental areas feedback strengths may depend on the base state because the amount of initial snow cover, for instance, is contingent on the control climate. Over tropical oceans cloud characteristics, and consequent radiative effects of clouds, could depend non-linearly on the absolute values of sea surface temperatures.

Cloud fraction changes in "amip4xCO2" are not confined to low clouds. In the tropics they most pronouncedly occur in the upper troposphere, while in other regions the vertical profile of cloud fraction changes is not robust across different climate models.

In summary, a component of tropospheric adjustment as diagnosed from the "amip4xCO2" experiment in computed feedbacks from transient climate simulations can not unequivocally be identified. Reasons may be the effects of land-sea contrast in the "amip4xCO2" experiments, inaccuracies in the kernel method to diagnose top-of-the atmosphere radiative flux anomalies due to cloud changes, or non-linearities of feedbacks (Mauritsen et al 2012). Although for some models tropospheric adjustment is present in the shortwave cloud feedback, and even dominant in the global mean, it is small in absolute terms, and the pattern correlation between radiative flux anomalies due to changes in clouds of "amip4K" and "1pctCO2" does not significantly increase in any of the models if the radiative flux anomalies from "amip4xCO2" are added to the ones from "amip4K".

Nevertheless, a positive correlation between the strength of tropospheric adjustment processes as diagnosed from the "amip4xCO2" experiment and cloud feedbacks can be ascertained across different climate models.

Acknowledgements Very valuable discussions with Bjorn Stevens, Levi Silvers, and Dagmar Popke are gratefully acknowledged. We thank all modeling groups who contributed data to CMIP5. The work was partially funded by the European Commission's 7th Framework Programme, under GA 226520 for the COMBINE project.

References

Andrews T, Gregory JM, Forster PM, Webb MJ (2011) Cloud adjustment and its role in CO_2 radiative forcing and climate sensitivity: a review. Surv Geophys DOI 10.1007/s10712-011-9152-0

Andrews T, Gregory JM, Webb MJ, Taylor KE (2012) Forcing, feedbacks and climate senisitivity in CMIP5 coupled atmosphere-ocean climate models. Geophys Res Lett 39, DOI 10.1029/2012GL051607

Block K, Mauritsen T (2012) Forcing and feedback in the MPI-ESM-LR coupled model under abruptly qudrupled CO_2, submitted to J. Adv. Model. Earth Syst.

Bony S, Dufresne JL (2005) Marine boundary layer clouds at the heart of tropical cloud feedback uncertainties in climate models. Geophys Res Lett 32, DOI 10.1029/2005GL023851

Bony S, Colman R, Kattsov VM, Allan RP, Bretherton CS, Dufresne JL, Hall A, Hallegatte S, Holland MM, Ingram W, Randall DA, Soden BJ, Tselioudis G, Webb MJ (2006) How well do we understand and evaluate climate change feedback processes? J Climate 19:3445–3482

Brient F, Bony S (2012) Interpretation of the positive low-cloud feedback predicted by a climate model under global warming. Climate Dyn DOI 10.1007/s00382-011-1279-7

Cess RD, Potter GL (1988) A methodology for understanding and intercomparing atmospheric climate feedback processes in general circulation models. J Geophys Res 93:8305–8314

Charba JP (1977) Operational system for predicting thunderstorms two to six hours in advance. Tech. Rep. 64, NOAA

Chylek P, Li J, Dubey MK, Wang M, Lesins G (2011) Observed and model simulated 20th century Arctic temperature variability: Canadian Earth System Model CanESM2. Atmos Chem Phys Discuss 11:22,893–22,907

Clement AC, Burgman R, Norris JR (2009) Observational and model evidence for positive low-level cloud feedback. Science 325:460–464

Climate System Modeling Division (2005) An introduction to the first-generation operational climate model at National Climate Center. No. 1 in Advances in Climate System Modeling

Clough SA, Shephard MW, Mlawer EJ, Delamere JS, Jacono MJ, Cady-Pereira K, Boukabara S, Brown PD (2005) Atmospheric radiative transfer modeling: a summary of the AER codes. J Quant Spectr Rad Transfer 91:233–244

Collins WD, Ramaswamy V, Schwarzkopf MD, Sun Y, Portmann RW, Fu Q, Casanova SEB, Dufresne JL, Fillmore DW, Forster PMD, Galin VY, Gohar LK, Ingram WJ, Kratz DP, Lefebvre MP, Li J, Marquet P, Oinas V, Tsushima Y, Uchiyama T, Zhong WY (2006) Radiative forcing by well-mixed greenhouse gases: Estimates from climate models in the Intergovernmental Panel on Climate Change (IPCC) Fourth Assessment Report (AR4). J Geophys Res 111, DOI 10.1029/2005JD006713

Colman R (2003) A comparison of climate feedbacks in general circulation models. Climate Dyn 20:865–873, DOI 10.1007/s00382-003-0310-z

Colman R, Fraser J, Rotstayn L (2001) Climate feedbacks in a general circulation model incorporating prognostic clouds. Climate Dyn 18:103–122, DOI 10.1007/s003820100162

Colman RA, McAvaney BJ (1997) A study of general circulation model climate feedbacks determined from perturbed sea surface temperature experiments. J Geophys Res 102:19,383–19,402

Colman RA, McAvaney BJ (2011) On tropospheric adjustment to forcing and climate feedbacks. Climate Dyn 36:1649–1658, DOI 10.1007/s00382-011-1067-4

Crueger T, Hohenegger C, May W (2012) Tropical precipitation and convection changes in the MPI-ESM in response to CO_2 forcing, submitted to J. Adv. Model. Earth Syst.

Del Genio AD, Kovari W (2002) Climatic properties of tropical precipitating convection under varying environmental conditions. J Climate 15:2597–2615

Dommenget D (2012) Analysis of the model climate sensitivity spread forced by mean sea surface temperature biases. J Climate DOI 10.1175/JCLI-D-11-00600.1

Dufresne JL, Bony S (2008) An assessment of the primary sources of spread of global warming estimates from coupled atmosphere-ocean models. J Climate 21:5135–5144

Dufresne JL, Foujols MA, Denvil S, Chaubel A, Marti O, Aumont O, Balkanski Y, Bekki S, Bellenger H, Benshila R, Bony S, Bopp L, Braconnot P, Brockmann P, Cadule P, Cheruy F, Codron F, Cozic A, Cugnet D, de Noblet N, Duvel JP, Ethé C, Fairhead L, Fichefet T, Flavoni S, Friedlingstein P, Grandpeix JY, Guez L, Guilyardi E, Hauglustaine D, Hourdin F, Idelkadi A, Ghattas J, Kageyama SJM, Krinner G, Lebetoulle S, Lehellec A, Lefebvre MP, Lefevre F, Levy C, Li ZX, Lloyd J, Lott F, Medec G, Mancip M, Marchand M, Masson S, Meurdesoif Y, Mignot J, Musat I, Parouty S, Polcher J, Rio C, Schulz M, Swingedouw D, Szopa S, Talandier C, Terray P, Viovy N (2012) Climate change projections using the IPSL-CM5 Earth System Model: from CMIP3 to CMIP5, submitted

Forster PM, Taylor KE (2006) Climate forcings and climate sensitivities diagnosed from coupled climate model integrations. J Climate 19:6181–6194

Fouquart Y, Bonnel B (1980) Computations of solar heating of the Earth's atmosphere: a new parametrization. Beitr Phys Atmos 53:35–62

Gent PR, Danabasoglu G, Donner LJ, Holland MM, Hunke EC, Jayne SR, Lawrence DM, Neale RB, Rasche PJ, Vertenstein M, Worley PH, Yang ZL, Zhang M (2011) The Community Climate System Model Version 4. J Climate 24:4973–4991

Gettelman A, Kay JE, Shell KM (2012) The evolution of climate sensitivity and climate feedbacks in the Community Atmosphere Model. J Climate 25:1453–1469

Giorgetta M, et al (2012) Climate variability and climate change in the MPI-ESM CMIP5 simulations, in preparation

Gregory JM, Mitchell JFB (1997) The climate response to CO_2 of the Hadley Centre coupled AOGCM with and without flux adjustment. Geophys Res Lett 24:1943–1946

Gregory JM, Webb M (2008) Tropospheric adjustment induces a cloud component in CO_2 forcing. J Climate 21:58–71

Hansen JE, Lacis A, Rind D, Russel G, Stone P, Fung I, Ruedy R (1984) Climate sensitivity: Analysis of feedback mechanisms. In: Hansen JE, Takahashi T (eds) Climate processes and climate sensitivity, Amer. Geophys. Union, pp 130–163

Held IM, Shell KM (2012) Using relative humidity as a state variable in climate feedback analysis. J Climate 25:2578–2582

Held IM, Soden BJ (2000) Water vapor feedback and global warming. Annu Rev Energy Environ 25:441–475

Jones CD, Hughes JK, Bellouin N, Hardiman SC, Jones GS, Knight J, Liddicoat S, O'Connor FM, Andres RJ, Bell C, Boo KO, Bozzo A, Butchart N, Cadule P, Corbin KD, Doutriaux-Boucher M, Friedlingstein P, Gornall J, Gray L, Halloran PR, Hurtt G, Ingram WJ, Lamarque JF, Law RM, Meinshausen M, Osprey S, Palin EJ, Chini LP, Raddatz T, Sanderson MG, Sellar AA, Schurer A, Valdes P, Wood N, Woodward S, Yoshioka M, Zerroukat M (2011) The HadGEM2-ES implementation of CMIP5 centennial simulations. Geosci Model Dev 4:543–570

Jonko AK, Shell KM, Sanderson BM, Danabasoglu G (2012) Climate feedbacks in CCSM3 under changing CO_2 forcing. Part I: Adapting the linear radiative kernel technique to feedback calculations for a broad range of forcings. J Climate 25:5260–5272

Kamae Y, Watanabe M (2012) Tropospheric adjustment to increasing CO_2: its timescale and the role of land-sea contrast. Clim Dyn DOI 10.1007/s00382-012-1555-1

Lambert FH, Webb MJ (2011) The relationship between land-ocean surface temperature contrast and radiative forcing. J Climate 24:3239–3256

Langen PL, Graversen RG, Mauritsen T (2012) Separation of contributions from radiative feedbacks to polar amplification on an aquaplanet. J Climate 25:3010–3024

Manabe S, Wetherald RT (1980) On the distribution of climate change resulting from an increase in CO_2 content of the atmosphere. J Atmos Sci 37:99–118

Mauritsen T, Graversen RG, Klocke D, Langen PL, Stevens B, Tomassini L (2012) Climate feedback efficiency and synergy, submitted to Climate Dynamics

Myhre G, Highwood EJ, Shine KP, Stordal F (1998) New estimates of radiative forcing due to well mixed greenhouse gases. Geophys Res Lett 25:2715–2718

Pethoukov V, Semenov VA (2010) A link between reduced Barents-Kara sea ice and cold winter extremes over northern continents. J Geophys Res 115, DOI 10.1029/2009JD013568

Rieck M, Nouijens L, Stevens B (2012) Marine boundary-layer cloud feedbacks in a constant relative humidity atmosphere. J Atmos Sci DOI 10.1175/JAS-D-11-0203.1

Seland O, Iversen T, Kirkevag A, Storelvmo T (2008) Aerosol-climate interactions in the CAM-Oslo atmsopheric GCM and investigation of associated basic shortcomings. Tellus A 60:459–491

Shell KM, Kiehl JT, Shields CA (2008) Using the radiative kernel technique to calculate climate feedbacks in NCAR's Community Atmospheric Model. J Climate 21:2269–2282

Sherwood SC, Ingram W, Tsushima Y, Satoh M, Roberts M, Vidale PL, O'Gorman PA (2010) Relative humidity changes in a warmer climate. J Geophys Res 115, DOI 10.1029/2009JD012585

Soden BJ, Held IM (2006) An assessment of climate feedbacks in coupled ocean-atmosphere models. J Climate 19:3354–3360

Soden BJ, Vecchi GA (2011) The vertical distribution of cloud feedback in coupled ocean-atmosphere models. Geophys Res Lett 38, DOI 10.1029/2011GL047632

Soden BJ, Held IM, Colman R, Shell KM, Kiehl JT, Shields CA (2008) Quantifying climate feedbacks using radiative kernels. J Climate 21:3504–3520

Stevens B, Crueger T, Esch M, Giorgetta M, Mauritsen T, Rast S, Schmidt H, Bader J, Block K, Brokopf R, Fast I, Kinne S, Kornblueh L, Lohmann U, Pincus R, Reichler T, Salzmann M, Röckner E (2012) The atmospheric component of the MPI Earth System Model: ECHAM6, in preparation

Tan J, Jakob C, Lane TP (2012) On the identification of the large-scale properties of tropical convection using cloud regimes, submitted to J. Climate

Taylor KE, Stouffer RJ, Meehl GA (2012) An overview of CMIP5 and the experiment design. Bull Amer Meteor Soc 93:485–498

Vecchi GA, Soden BJ (2007) Global warming and the weakening of the tropical circulation. J Climate 20:4316–4340

Voldoire A, Sanchez-Gomez E, Salas y Mélia D, Decharme B, Cassou C, Sénési S, Valcke S, Beau I, Alias A, Chevallier M, Déqué M, Deshayes J, Douville H, Fernandez E, Madec G, Maisonnave E, Moine MP, Planton S, Saint-Martin D, Szopa S, Tyteca S, Alkama R, Belamari S, Coquart L, Chauvin F (2012) The CNRM-CM5.1 global climate model: description and basic evaluation. Clim Dyn DOI 10.1007/s00382-011-1259-y

Volodin EM, Dianskii NA, Gusev AV (2010) Simulating present-day climate with the INMCM4.0 coupled model of the atmospheric and oceanic general circulation. Izv, Atmos Ocean Phys 46:414–431

Watanabe M, Suzuki T, O'ishi R, Komuro Y, Watanabe S, Emori S, Takemura T, Chikira M, Ogura T, Sekiguchi M, Takata K, Yamazaki D, Yokohata T, Nozawa T, Hasumi H, Tatebe

H, Kimoto M (2010) Improved climate simulation by MIROC5: mean states, variability, and climate sensitivity. J Climate 23:6312–6335
Watanabe M, Shiogama H, Yoshimori M, Ogura T, Yokohata T, Okamoto H, Emori S, Kimoto M (2011) Fast and slow timescales in the tropical low-cloud response to increasing CO_2 in two climate models. Clim Dyn DOI 10.1007/s00382-011-1178-y
Webb MJ, Lambert FH, Gregory JM (2012) Origins of differences in climate sensitivity, forcing and feedback in climate models. Climate Dyn DOI 10.1007/s00382-012-1336-x
Wetherald RT, Manabe S (1988) Cloud feedback processes in a general circulation model. J Atmos Sci 45:1397–1415
Winton M, Takahashi K, Held IM (2010) Importance of ocean heat uptake efficacy to transient climate change. J Climate 23:2333–2344
Wood R, Bretherton CS (2006) On the relationship between stratiform low cloud cover and lower-tropospheric stability. J Climate 19:6425–6432
Wyant MC, Bretherton CS, Blossey PN, Khairoutdinov M (2012) Fast cloud adjustment to increasing CO_2 in a superparameterized climate model. J Adv Model Earth Syst 4, DOI 10.1029/2011MS000092
Yukimoto S, Yoshimura H, andT Sakami MH, Tsujino H, Hirabara M, Tanaka TY, Deushi M, Obata A, Nakano H, Adachi Y, Shindo E, Yabu S, Ose T, Kitoh A (2011) Meteorological Research Institute-Earth System Model Version 1 - Model description. Tech. Rep. 64, Meteorological Research Institute
Zelinka MD, Hartmann DL (2010) Why is longwave cloud feedback positive? J Geophys Res 115, DOI 10.1029/2010JD013817
Zelinka MD, Klein SA, Hartmann DL (2012a) Computing and partitioning cloud feedbacks using cloud property histograms. Part I: cloud radiative kernels. J Climate 25:3715–3735
Zelinka MD, Klein SA, Hartmann DL (2012b) Computing and partitioning cloud feedbacks using cloud property histograms. Part II: attribution to changes in cloud amount, altitude, and optical depth. J Climate 25:3736–3754
Zhang MH, Hack JJ, Kiehl JT, Cess RD (1994) Diagnostic study of climate feedback processes in atmospheric general circulation models. J Geophys Res 99:5525–5537
Zhang Y, Stevens B, Medeiros B, Ghil M (2009) Low-cloud fraction, lower-tropospheric stability, and large-scale divergence. J Climate 22:4827–4844

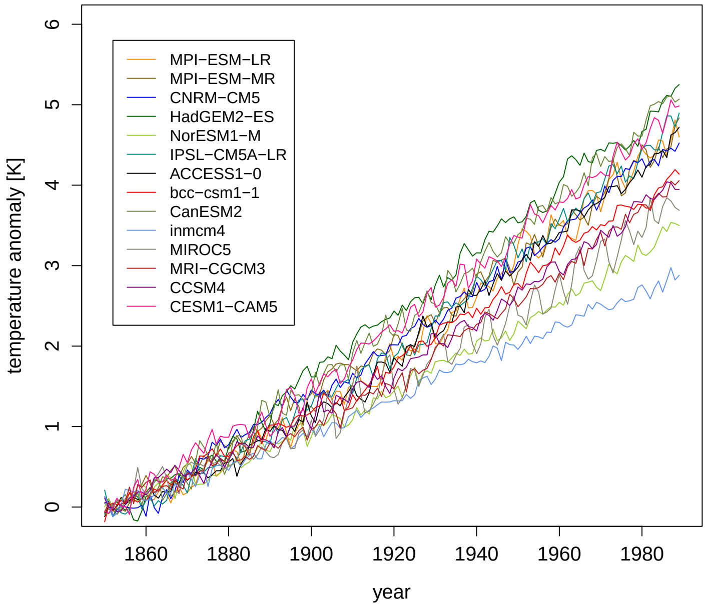

Fig. 1 The global mean temperature increase in the "1pctCO2" experiment for the 14 models considered in the present study. Anomalies are computed with respect to the pre-industrial control simulation.

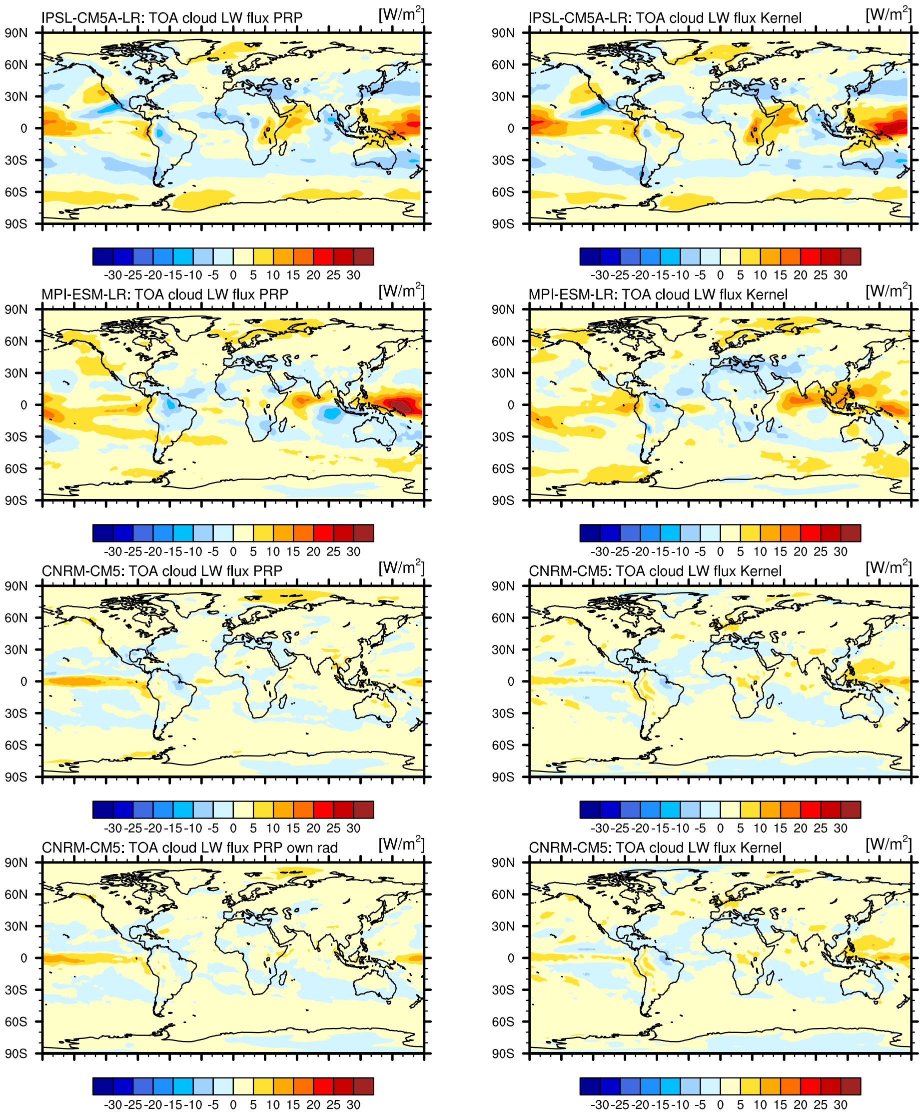

Fig. 2 Top-of-the-atmosphere longwave fluxes due to changes in clouds derived from partial radiative perturbation (PRP) calculations (left column) and a radiative kernel (right column) for three different CMIP5 models. In the case of CNRM-CM5 the PRP computations are performed with the ECHAM6 off-line radiation code (third row) as well as with the native radiation scheme of the model (fourth row).

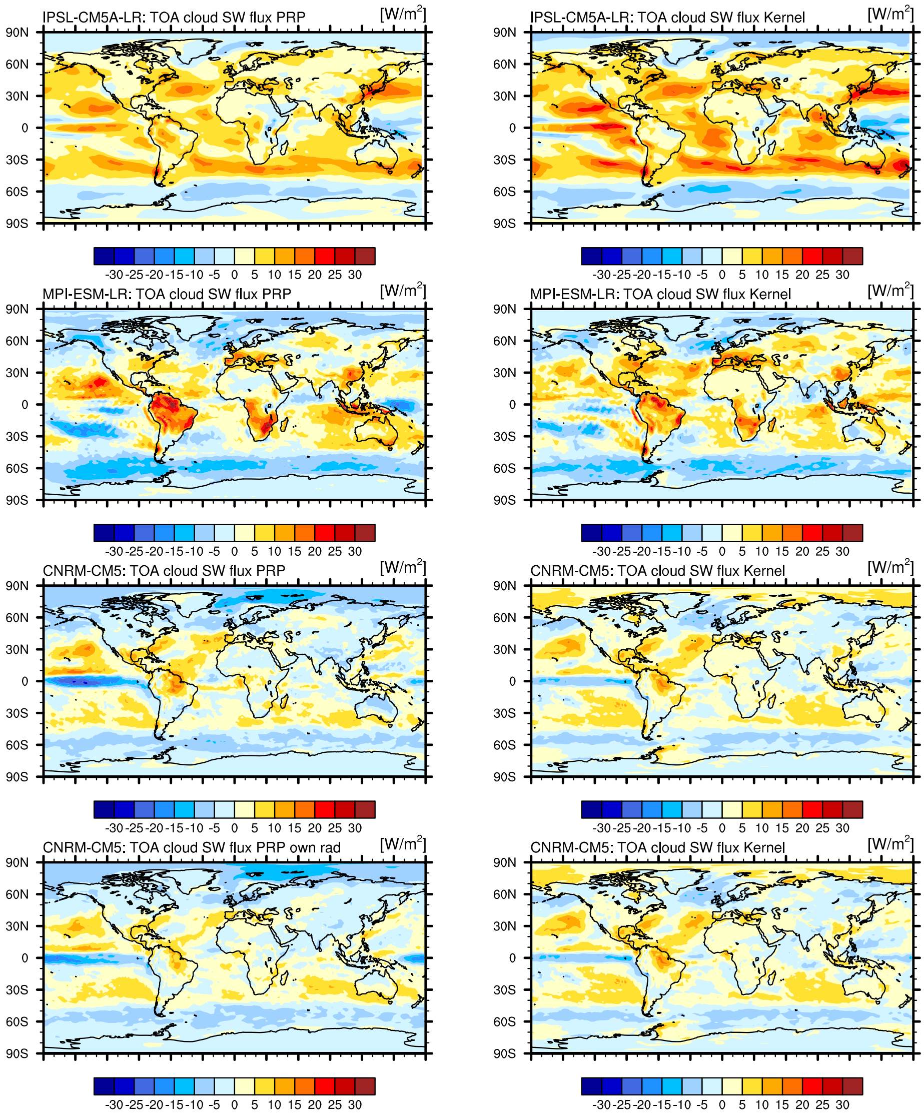

Fig. 3 Top-of-the-atmosphere shortwave fluxes due to changes in clouds derived from partial radiative perturbation (PRP) calculations (left column) and a radiative kernel (right column) for three different CMIP5 models. In the case of CNRM-CM5 the PRP computations are performed with the ECHAM6 off-line radiation code (third row) as well as with the native radiation scheme of the model (fourth row).

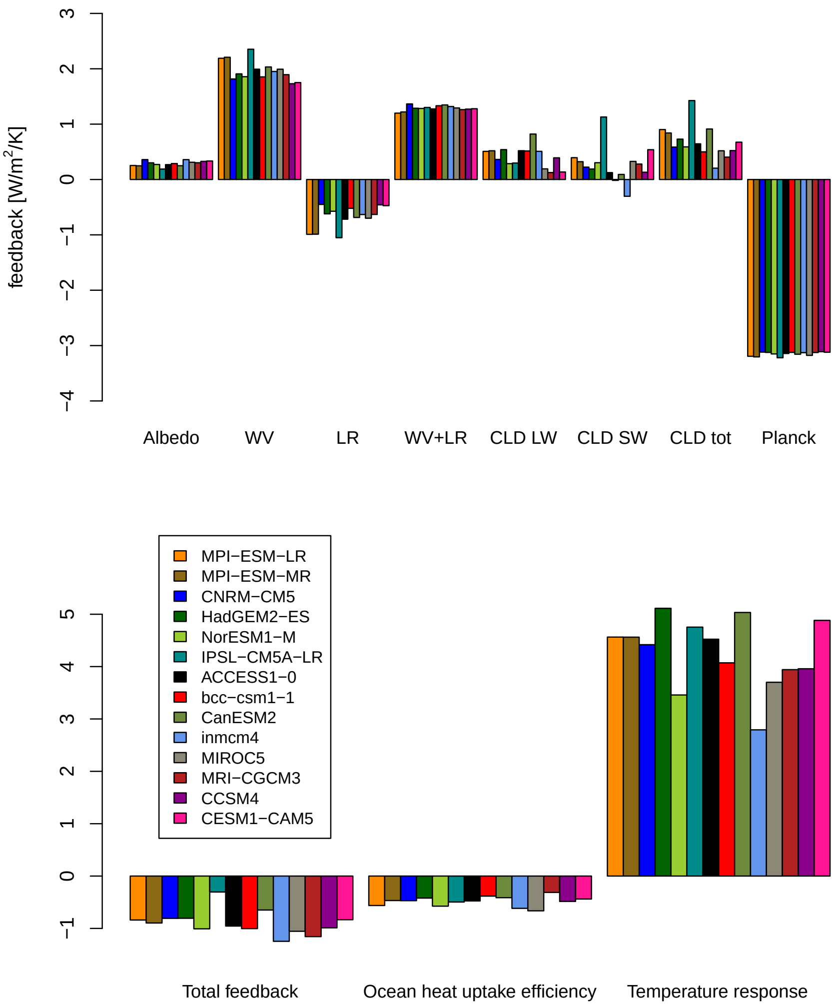

Fig. 4 Upper panel: albedo, water vapor, lapse rate, joint water vapor and lapse rate, cloud longwave, cloud shortwave, total cloud, and Planck feedback for 14 CMIP5 climate models diagnosed from the "1pctCO2" simulation. Lower panel: total feedback, ocean heat uptake efficiency κ, and amplitude of the surface temperature response in the "1pctCO2" experiment for all the models. Here the kernel method was used for the computation of the various feedbacks.

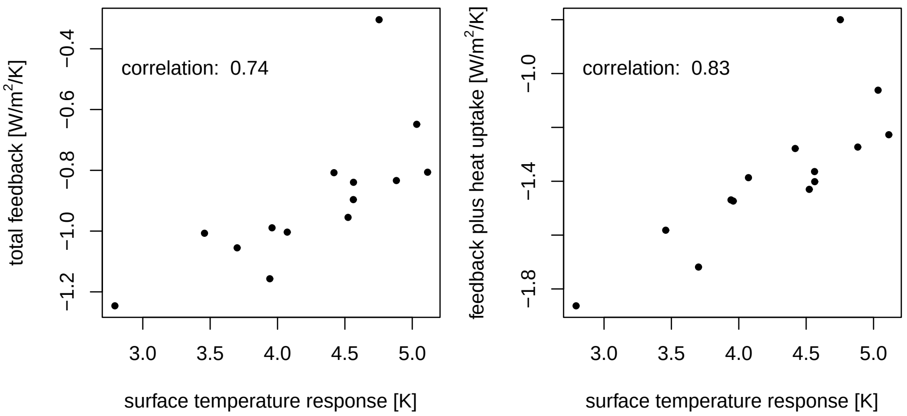

Fig. 5 Left panel: scatter plot of surface temperature response against total feedback factors for the 14 climate models. Right panel: scatter plot of surface temperature response against total feedback plus ocean heat uptake efficiency for the same climate models.

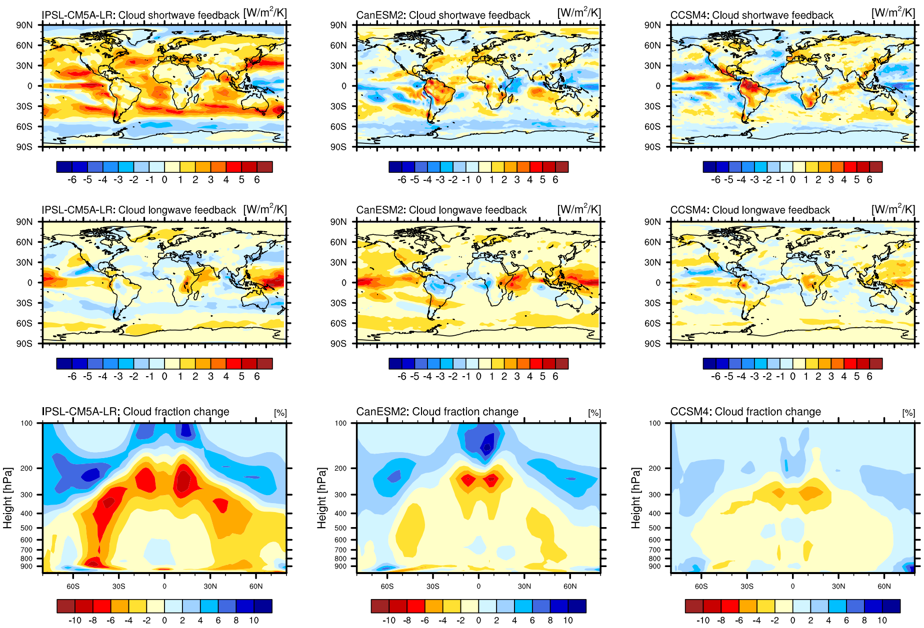

Fig. 6 Cloud shortwave (first row) and cloud longwave (second row) feedbacks for three CMIP5 models. The third row shows zonal mean cloud fraction changes for the same models.

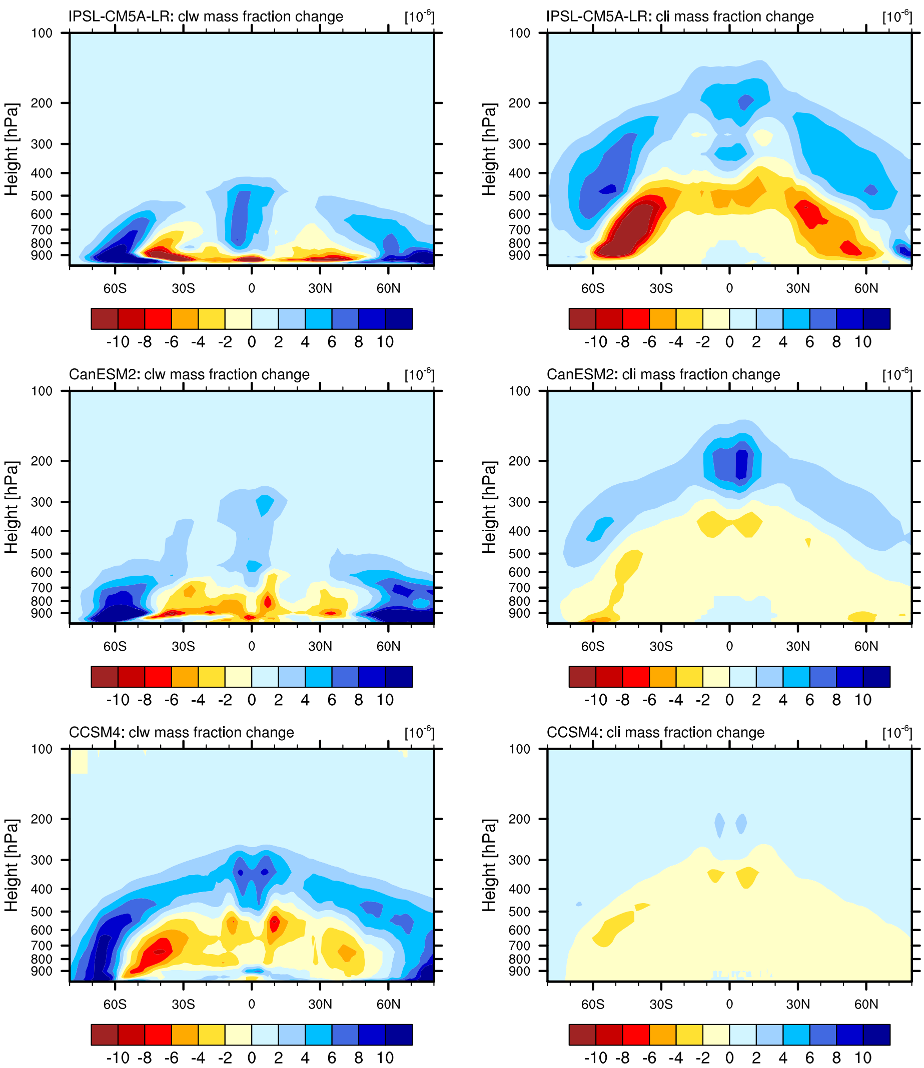

Fig. 7 Zonal mean changes in cloud liquid water (left column) and cloud ice (right column) for three CMIP5 models. The climate models are the same as in Figure 6.

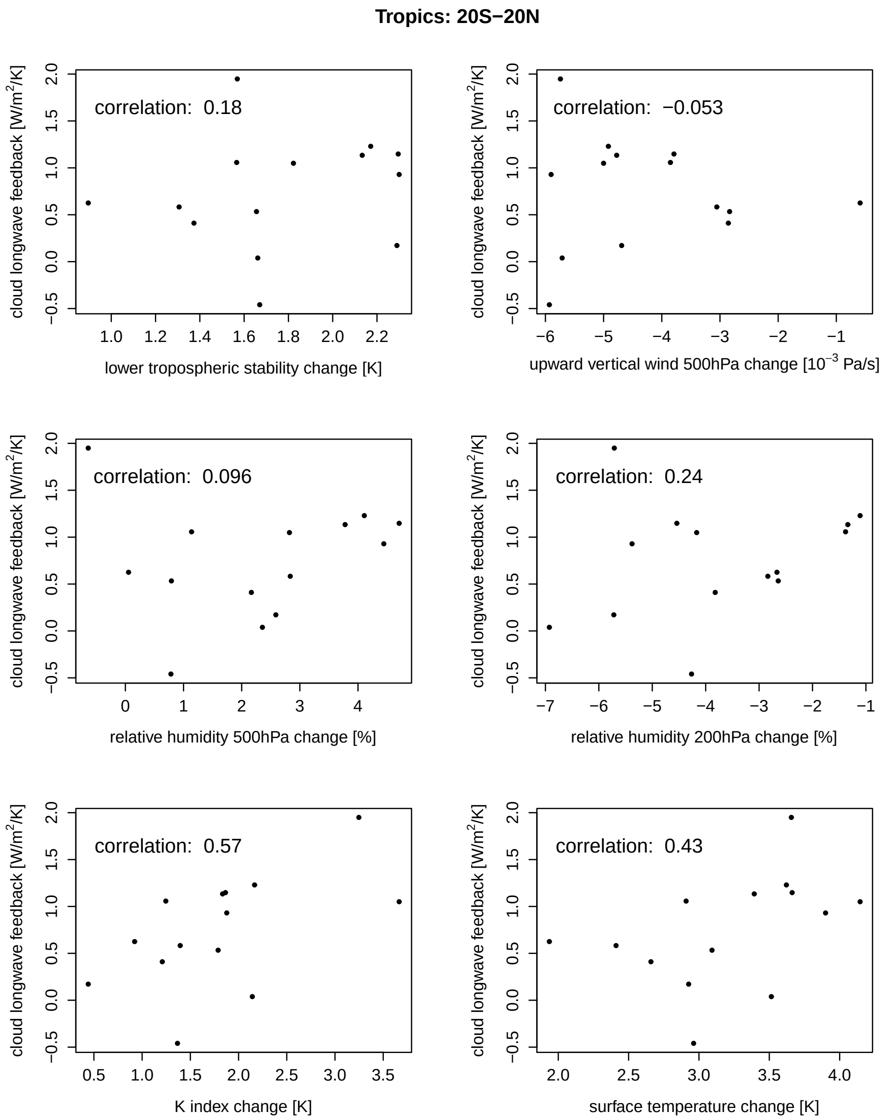

Fig. 8 Scatter plot of cloud longwave feedback and changes in different large-scale indices over the tropical region of 20 South to 20 North: lower tropospheric stability, upward vertical wind at 500hPa, relative humidity at 500hPa and 200hPa, a convection index, and surface temperature. The convection index is the modified K-index defined by Charba (1977). All indices are restricted to ocean areas except for the upward vertical wind which includes also the land parts of the region.

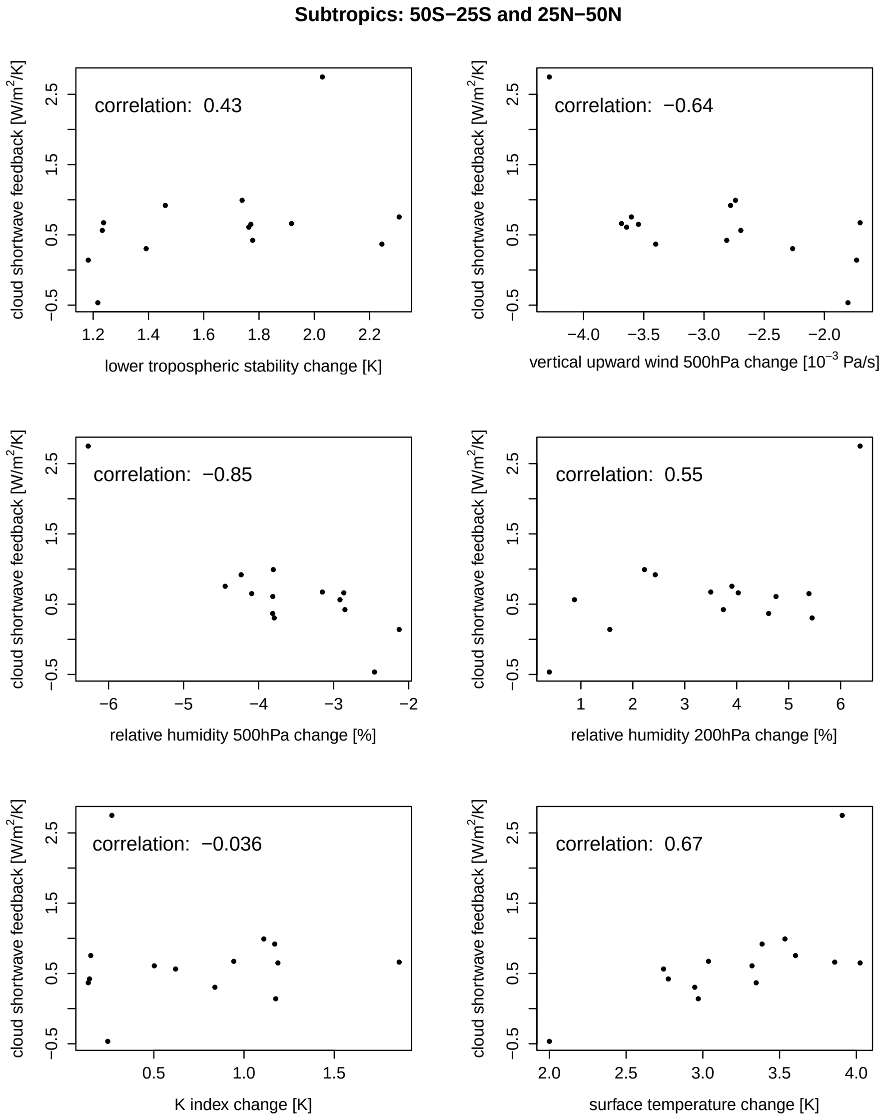

Fig. 9 Scatter plot of cloud shortwave feedback and changes in different large-scale indices over the subtropical region of 50 South to 25 South and 25 North to 50 North: lower tropospheric stability, upward vertical wind at 500hPa, relative humidity at 500hPa and 200hPa, a convection index, and surface temperature. The convection index is the modified K-index defined by Charba (1977). All indices are restricted to ocean areas except for the upward vertical wind which includes also the land parts of the region.

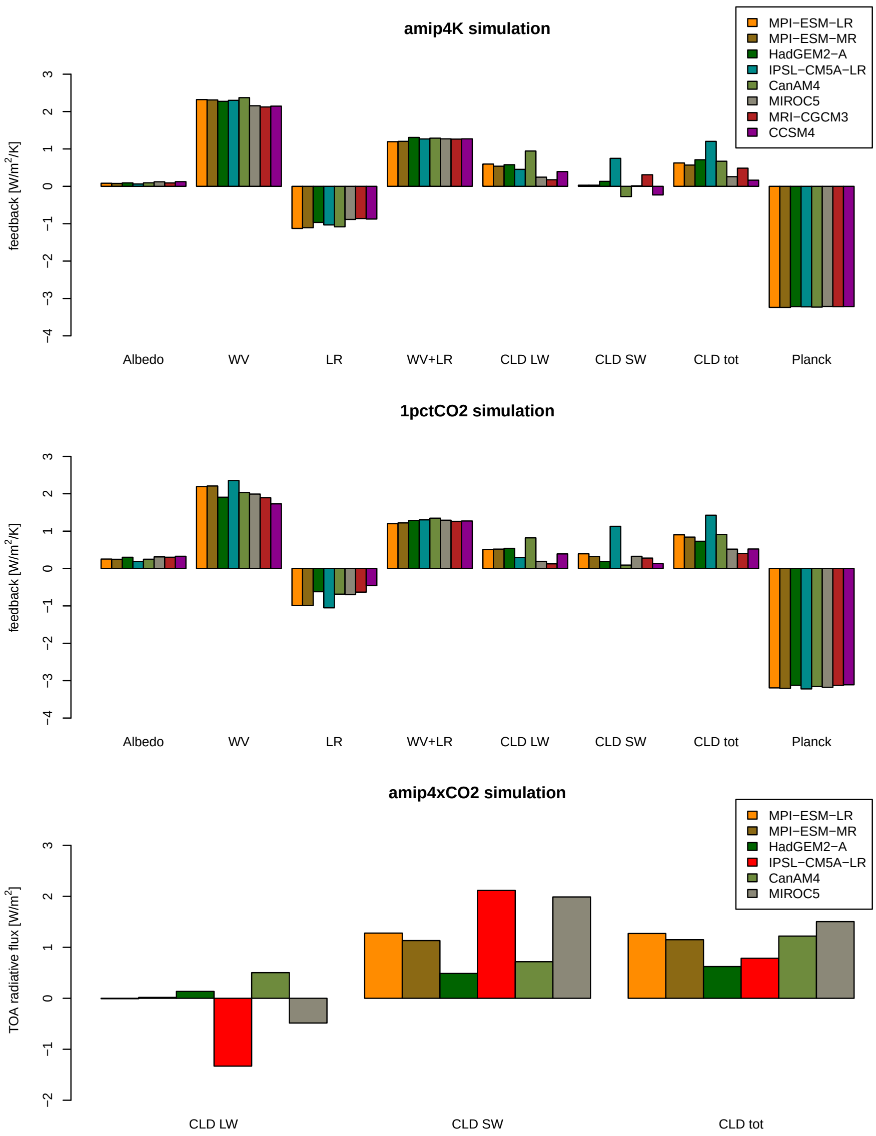

Fig. 10 Upper panel: albedo, water vapor, lapse rate, joint water vapor and lapse rate, cloud longwave, cloud shortwave, total cloud, and Planck feedback for 8 CMIP5 climate models diagnosed from the "amip4K" experiment. Middle panel: the same feedbacks for the same models as computed from the "1pctCO2" simulation (identical to the ones in Figure 4). Lower panel: longwave, shortwave, and the sum of longwave and shortwave top-of-the-atmosphere fluxes due to changes in clouds for 6 CMIP5 models as diagnosed from the "amip4xCO2" experiment.

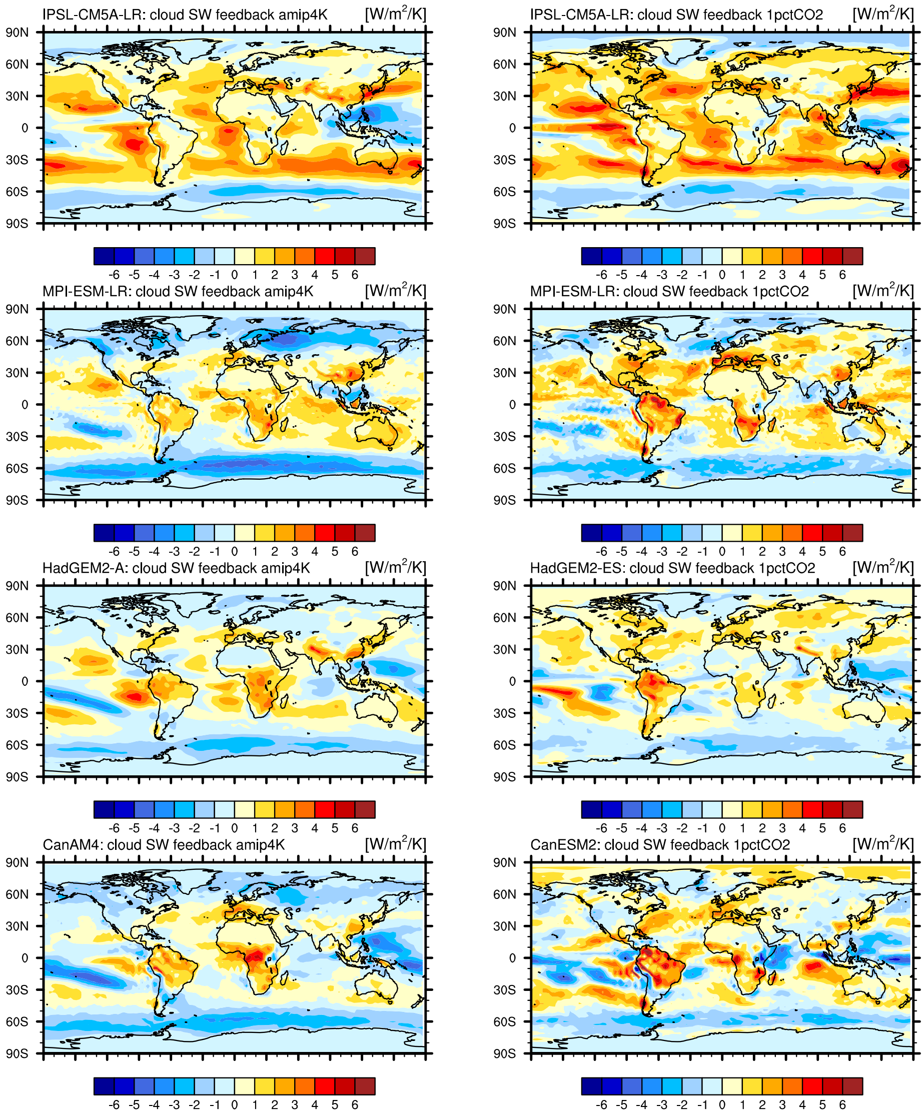

Fig. 11 Cloud shortwave feedbacks diagnosed from the "amip4K" (left column) and the "1pctCO2" (right column) experiment for four CMIP5 models.

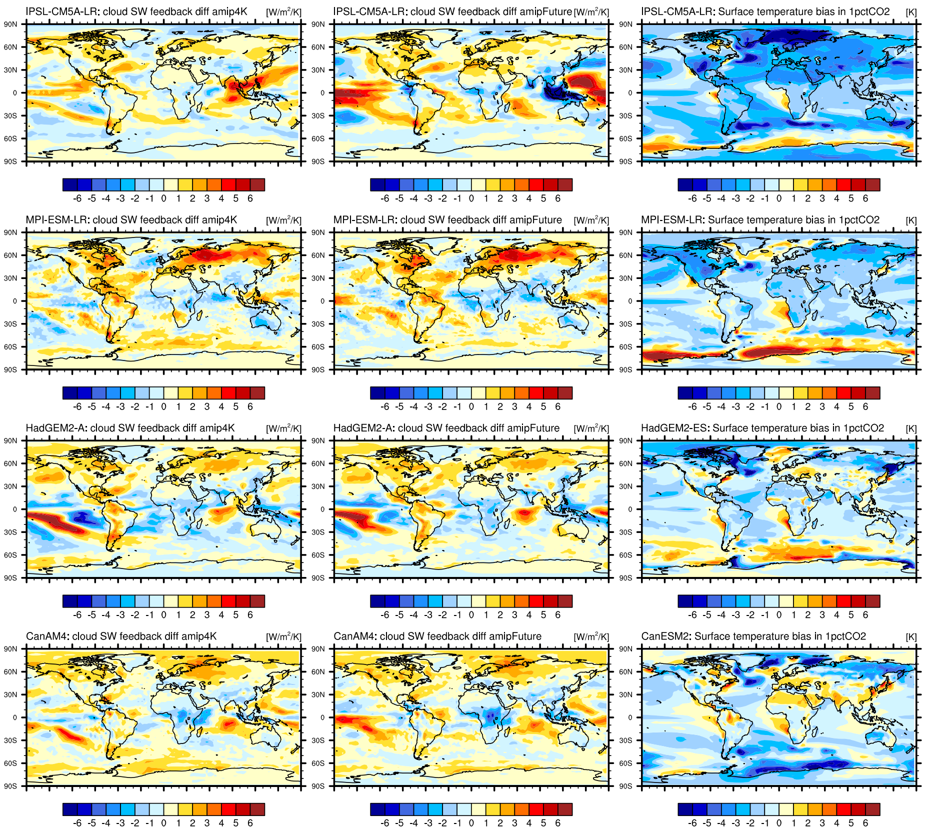

Fig. 12 Left column: difference of the cloud shortwave feedback from "1pctCO2" and "amip4K" for four CMIP5 models. Middle column: difference of the cloud shortwave feedback from "1pctCO2" and "amipFuture" for the same models. Right column: difference of surface temperatures in the control state of "1pctCO2" (i.e. the mean over the first six years of "1pctCO2") and in the control state of the AMIP-type experiments (i.e. the mean over the 30 years of the standard "amip" simulation) for the four models.

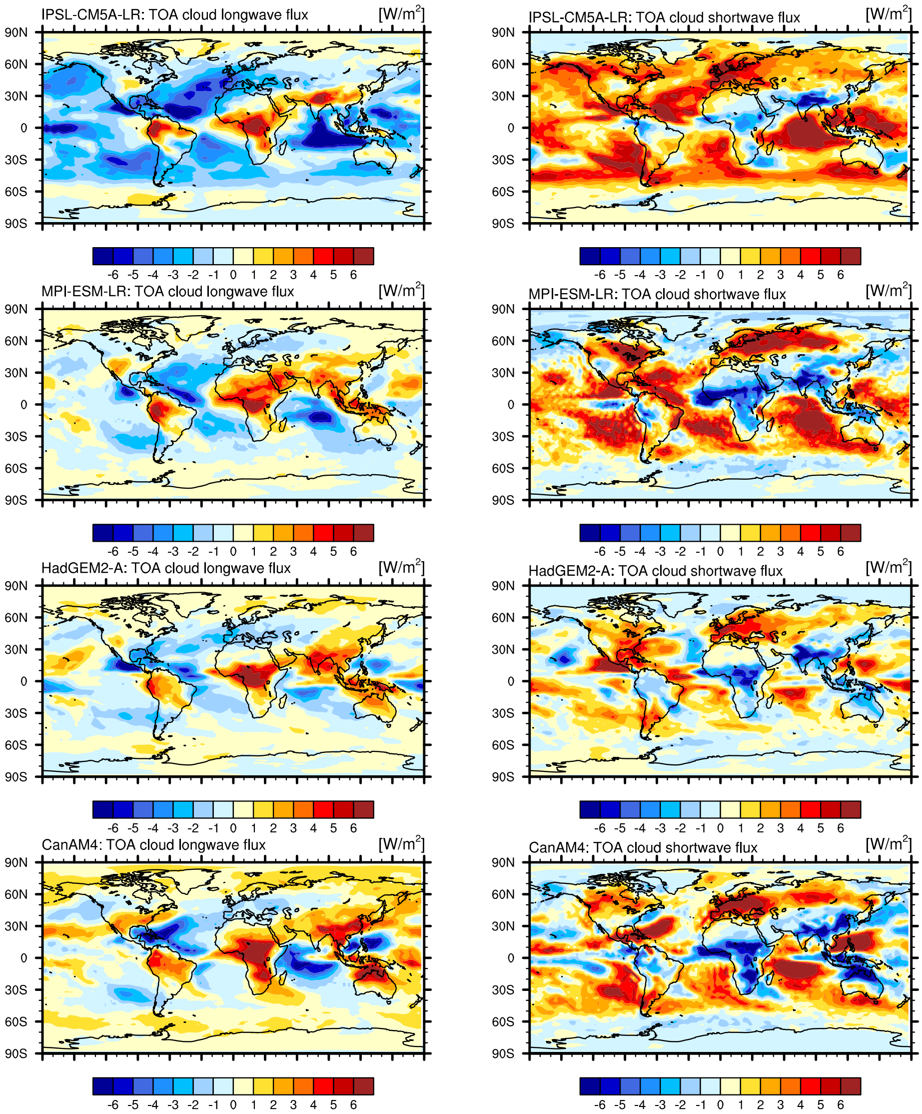

Fig. 13 Top-of-the-atmosphere longwave (left column) and shortwave (right column) fluxes due to changes in clouds computed from the "amip4xCO2" experiment for 4 CMIP5 models.

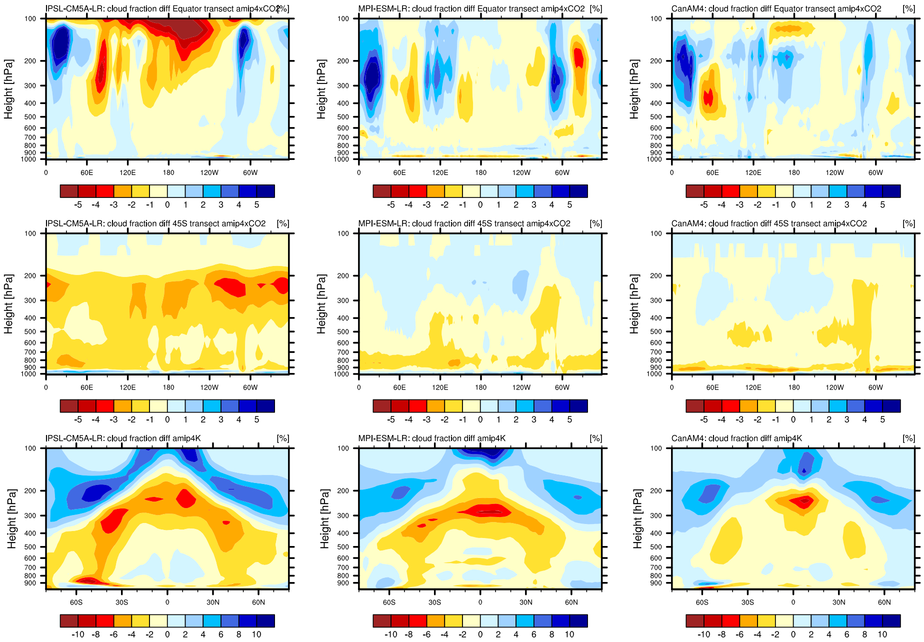

Fig. 14 First row: cloud fraction changes in the "amip4xCO2" experiment along the Equator (i.e. between 5 South and 5 North) for three CMIP5 models. Second row: cloud fraction changes in the "amip4xCO2" experiment along 45 South (i.e. between 50 South and 40 South) for the same models. Third row: zonal mean cloud fraction changes in the "amip4K" experiment for the three models.

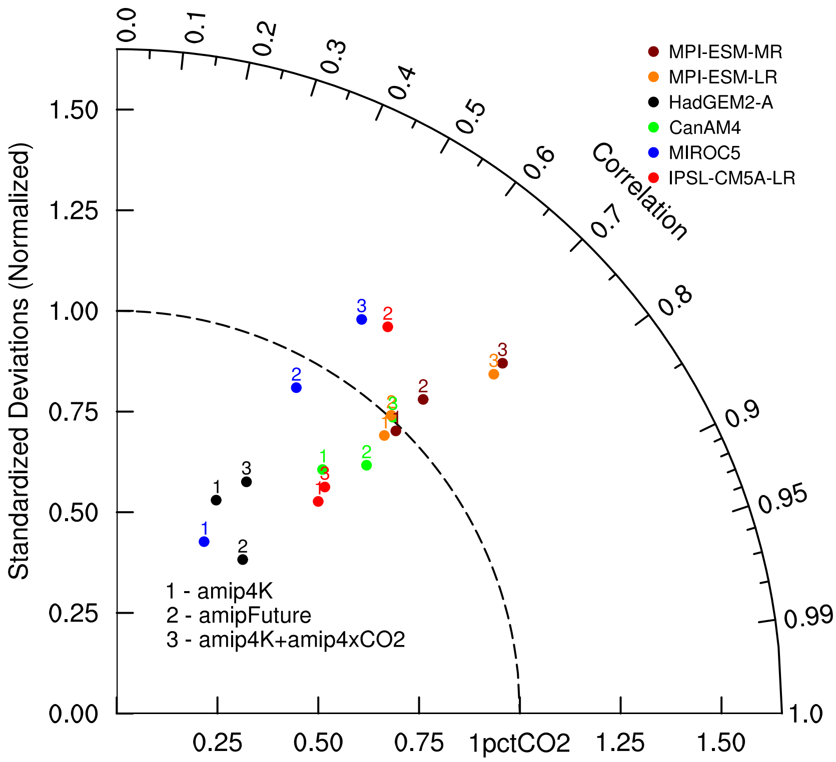

Fig. 15 Comparison of top-of-the-atmosphere total radiative flux anomalies due to changes in clouds from different experiments with the ones from "1pctCO2" for 6 CMIP5 models. The experiments are "amip4K", "amipFuture", and "amip4K+amip4xCO2" (i.e. the flux anomalies of "amip4xCO2" are added to ones from "amip4K"). The reference experiment is "1pctCO2". The Taylor diagram comprises the variances of the fields (relative to the reference experiment) and the pattern correlations with the reference simulation. The flux anomalies from "amip4K" and "amipFuture" are scaled by the ratio of the global mean temperature increase in these experiments and the global mean temperature change in "1pctCO2".

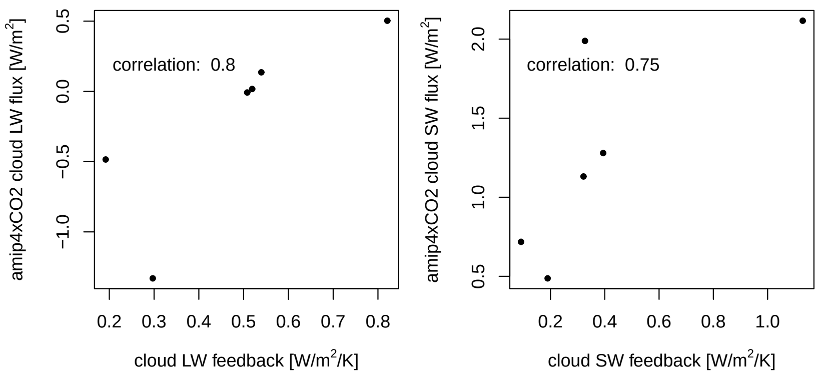

Fig. 16 Left panel: scatter plot of longwave cloud feedbacks diagnosed from the "1pctCO2" experiment against top-of-the-atmosphere longwave flux anomalies due to changes in clouds from "amip4xCO2". Right panel: scatter plot of shortwave cloud feedbacks diagnosed from the "1pctCO2" experiment against top-of-the-atmosphere shortwave flux anomalies due to changes in clouds from "amip4xCO2" for the respective models.